Figure 10. The regional Bouguer anomaly map at a scale of 1 to 50,000, which is created by using the data aquired in the program CG-01, is shown Figure in 11.

Relative gravity to that at the known station is measured using a gravimeter, Model D with a detection accuracy of 0.1 μgal, manufactured by La Coste & Romberg Co., Ltd. The gravity base station ST1000 of the current survey is set at the courtyard of the Emir hotel in Gâafour located in the south of the current prospects. ST1000's gravity value is desided by using relative mersurement between the bases of the ONM gravity program CG-02 ant it. Gravity is measured once or more every day at the gravity base station for each closing gravity traverse. The maximum error for one closing gravity traverse is recorded at 0.1 mgal throughout the current survey.

A gravity value, *ABSG* (mgal), at each measuring station is estimated using a relative gravity, *RG*, at the measuring point and the gravity value, *ABSG*, at the gravity base station as follows;

$$ABSG(measuring\ point) = RG(measuring\ station) - RG(base) + ABSG(base) \quad (1)$$

where,

$$RG = reading * factor + C_{inst} + C_{tidal} + C_{drift} \quad (2)$$

reading: instrumental reading, *factor*: reading−coefficient of conversion

C_{inst}: correction for instrument height, C_{tidal}: tidal correction

C_{drift}: drift correction.

A Bouguer gravity value, *Ab* (mgal), is also estimated for each measured gravity value (*ABSG*) using the following equation;

$$Ab = ABSG - G_{stand}(\phi) + C_{atm}(h) + C_{free}(h) + Cb(h, \gamma) + T(h, \gamma) \quad (3)$$

ϕ: latitude of measuring point, h: elevation of measuring point(m)

γ: specific gravity of rocks in the vicinity of measuring point(g/cm^3)

where

- Standard Gravity Value (1967 formula)

$$G_{stand}(\phi) = 978031.85(1+0.005278895 \sin^2 \phi + 0.000023462 \sin^4 \phi) \quad (4)$$

- Atmospheric Correction

$$C_{atm}(h) = 0.87 - 0.000965\, h \quad (5)$$

- Free-air Correction

$$C_{free}(h) = (\partial g / \partial h)\, h = 0.3086\, \mathrm{h} \quad (6)$$

- Bouguer Correction

$$Cb(h, \gamma) = -2\pi G \gamma h = -0.04192 \gamma h \quad (7)$$

π: circular constant, G: universal gravitation constant

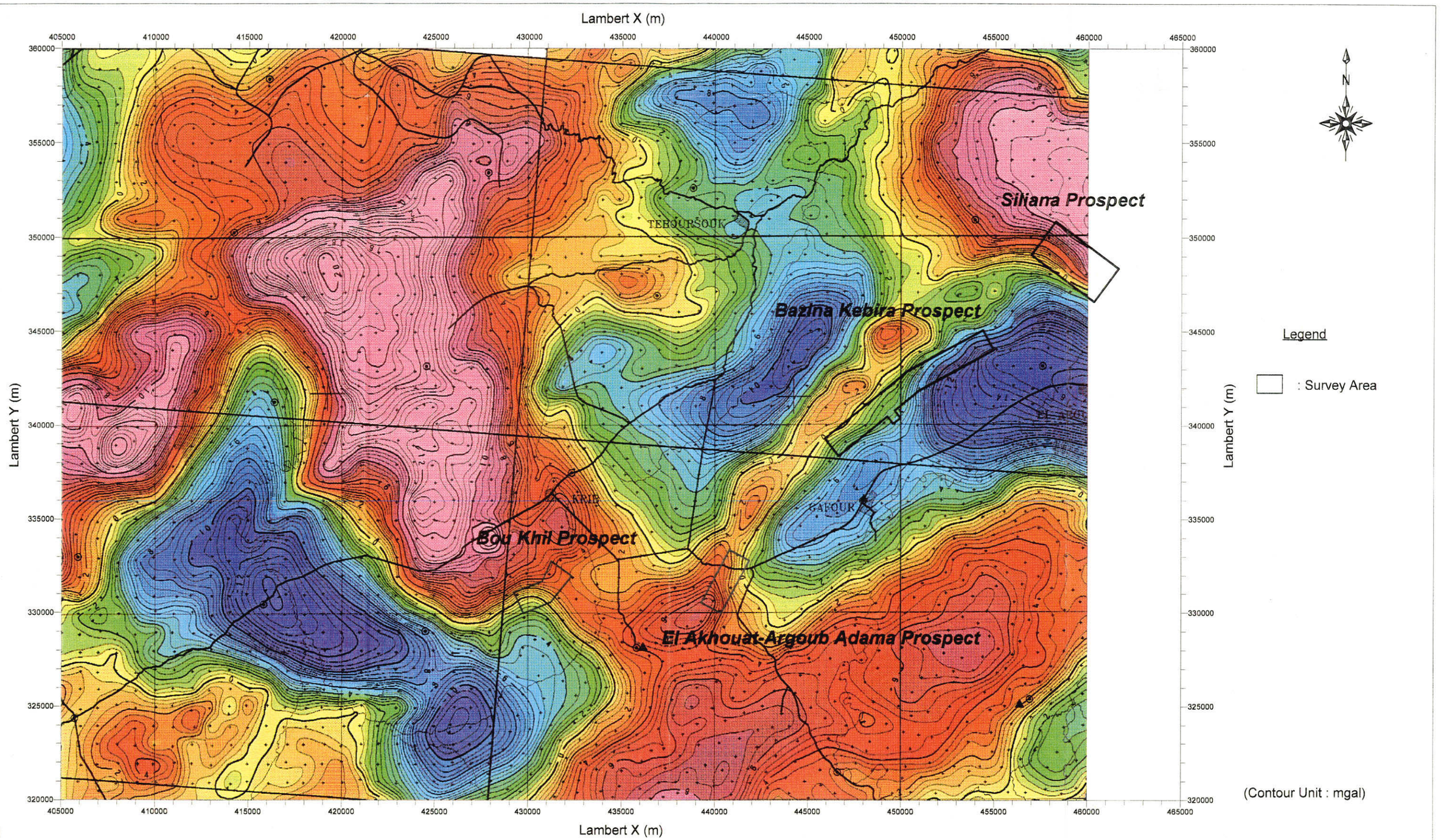

Part of ONM, 1999

Figure 10
Regional gravity map (Density : 2.33 g/cm^3)
Scale 1 : 200,000
March, 2001

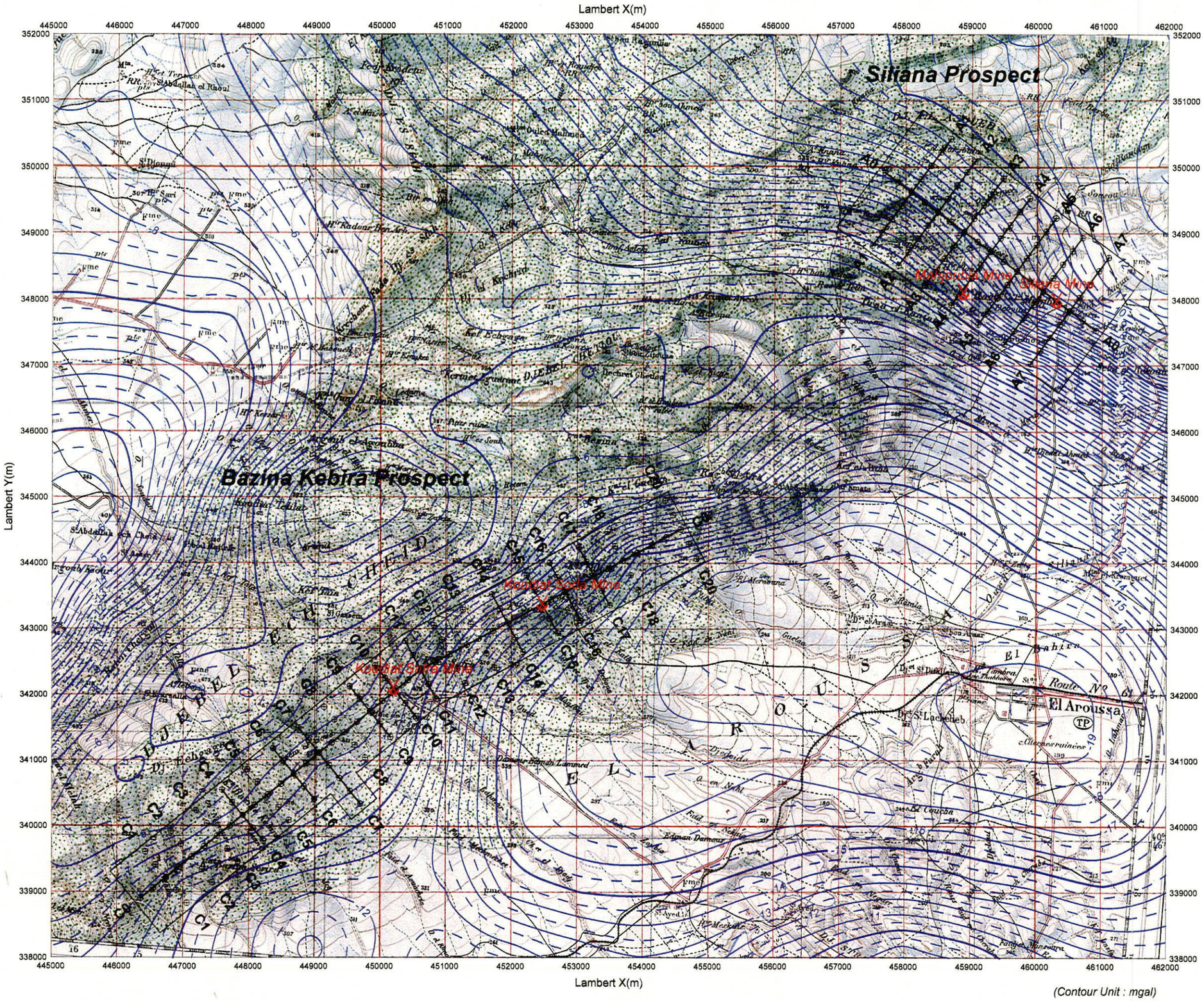

Figure 11

Regional bouguer anomaly map
(Density : 2.4 g/cm³)

Scale 1 : 60,000

March, 2001

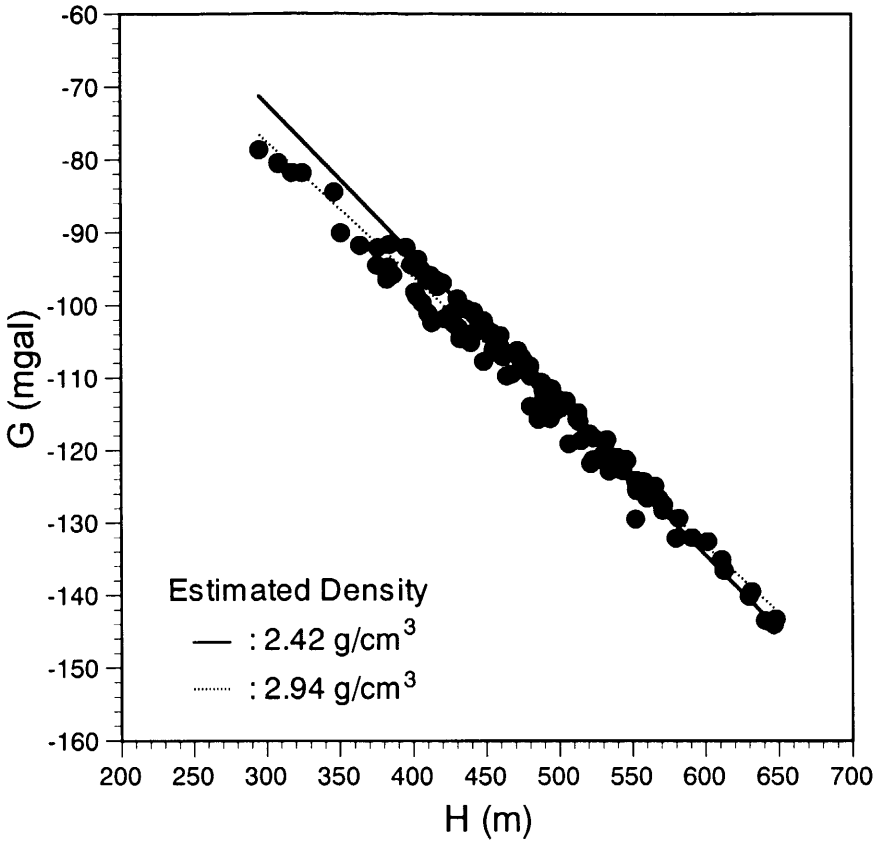

(a) Bazina Kebira prospect

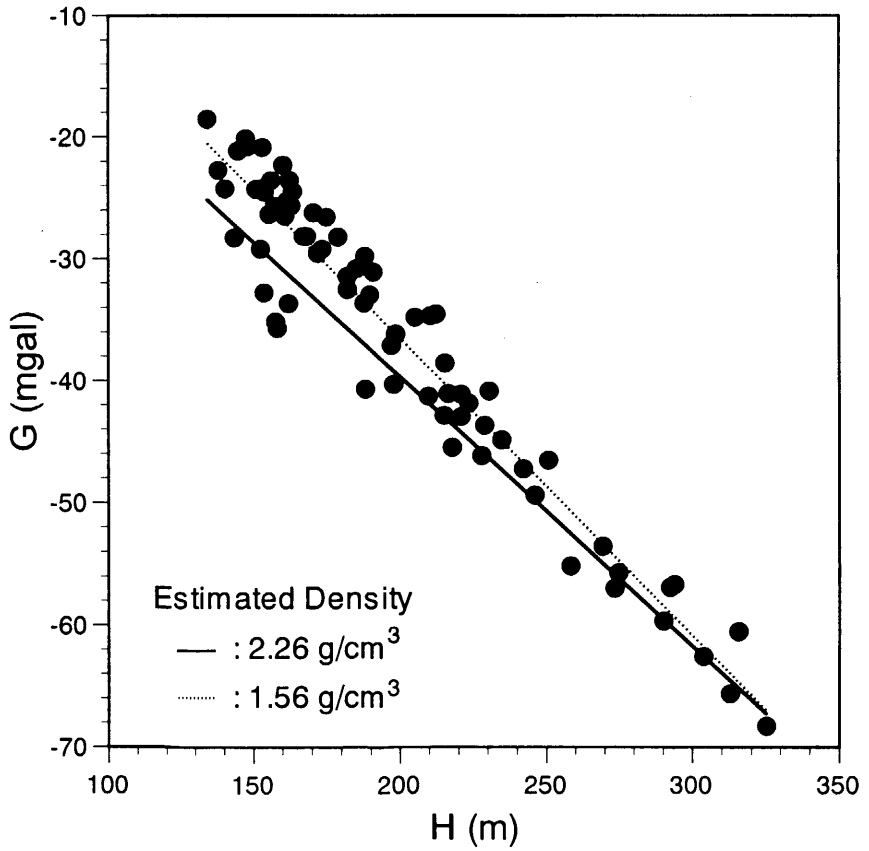

(b) Siliana prospect

Figure 12 G - H correlation diagram

- Topographic Correction: T(h, γ)

  adopting the Topographic Correction Formula of GSJ (Geological Survey of Japan), established in 1989 by its Gravity Survey Research Group.

The density in the vicinity of measuring stations, which is used for the Bouguer and topographic corrections, is usually determined by an appropriate judgement taking account of densities estimated according to the following means;

① the result of density measurement of rock samples.

② the gradient of G-H correlation diagram.

G-H correlation diagram (Figure 12): produced by plotting measurements on a diagram with the abscissa for the differences between measured and standard gravity values against the ordinate for the elevation differences between measuring points.

③ comparison of the topographic map with Bouguer anomaly maps for several assumed densities: selecting the density least correlated to the topography.

The average of density measurement of rock samples collected in and near the current prospects is 2.60 g/cm^3. A density of 2.42 g/cm^3 is obtained on the basis of the G-H diagrams for the Bazina Kebira prospect and a density of 2.26 g/cm^3 for the Siliana prospect. Besides, the Bouguer anomaly maps for the densities of 2.3 and 2.4 are judged to be relatively low in their correlativity with the topographic map. Taking these results into consideration, the correction densities of 2.4 g/cm^3 for the Bazina Kebira prospect and 2.3 g/cm^3 for the Siliana prospect are adopted in the current gravity survey for the purpose of comparison.

Horizontal distribution of Bouguer gravity values comprises composite of shorter and longer spatial wavelength variations of gravity in the region as illustrated in Figure 13. The shorter wavelength variation reflects density variation of rocks in the shallower part of earth and the longer wavelength variation, that in the deeper part, several kilometers or deeper from the surface. The Bouguer gravity values of the current prospects, after estimation of 2-dimensional Fourier transform, are plotted on the power spectrum diagram (Figure 14) with the abscissa for wave number (spatial frequency) against the ordinate for natural logarithm of spectrum power. According to the diagram, the Bouguer gravity anomaly of the Bazina Kebira prospect is composed of three components with their average depths at 1,119 m, 169 m and 44 m. The Bouguer gravity anomaly of the Bazina Kebira prospect is also composed of three components with their average depths at 762 m, 154 m and 44 m. Since the current gravity survey is concerned with prospecting ore deposits shallower than a few kilometers, it is tried to extract a shorter wavelength, that is, shallow component from the Bouguer anomaly map.

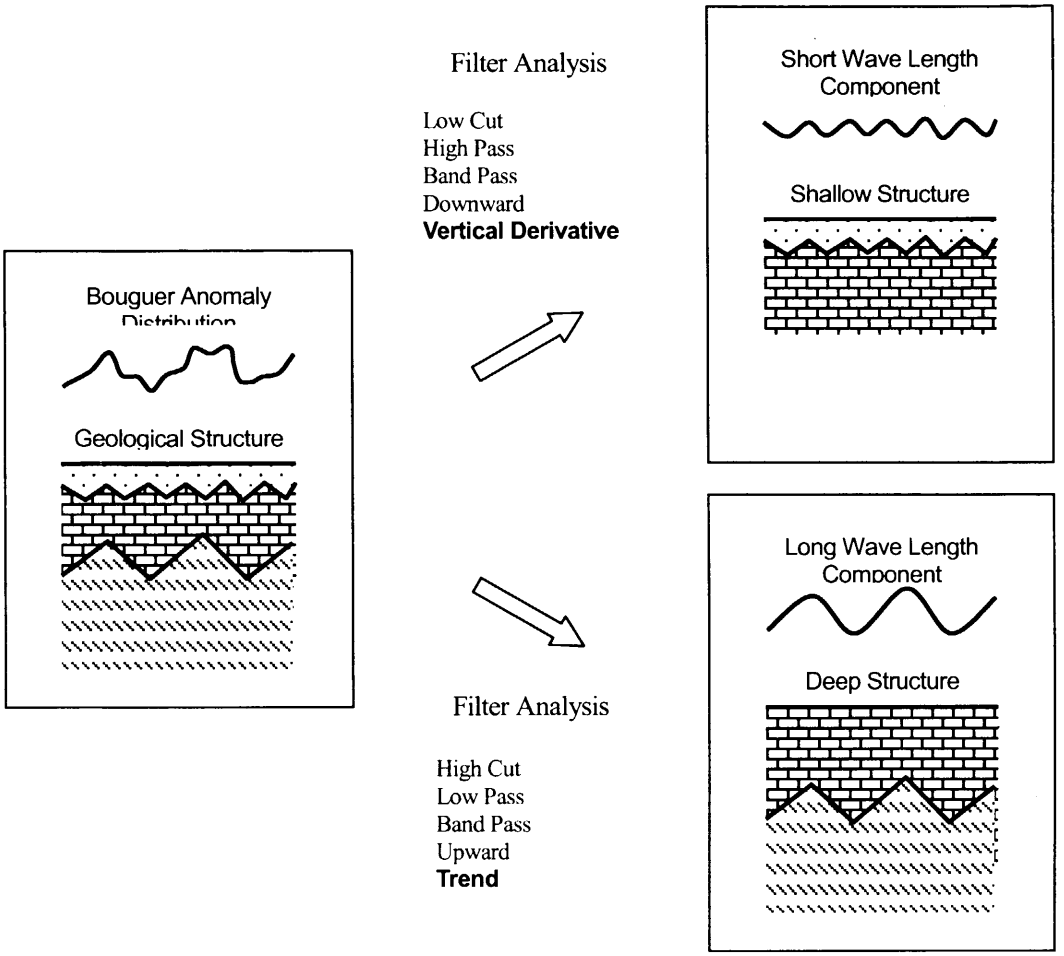

Figure 13 Schematic Diagram of Filter Analysis in Gravimetric Surveys

For extracting the shorter wavelength component, one approach is to use a low-cut or band-pass filter for data processing and the other, to estimate residuals over a regional trend surface of Bouguer gravity values. In the current survey, the first vertical derivative filter, a kind of low-cut filter, and the trend surface analysis are adopted for extracting the shorter wavelength component.

The result of first vertical derivative filtering is shown in the first vertical derivative anomaly map. The 0 contour between the positive maximum and the negative minimum indicates a boundary between two subsurface geologic bodies with different density structures, e.g. a fault, a intrusive contact, etc., as shown in Figure 15.

In general, a trend surface is mathematically approximated by an n-dimensional polynomial or is obtained using a low-pass filter such as the upward continued filter. Where measuring stations are sparsely located, the shorter wavelength component tends to be also filtered out. Therefore, the Bouguer anomaly distribution of the CG-01 Project (Figure 11), in

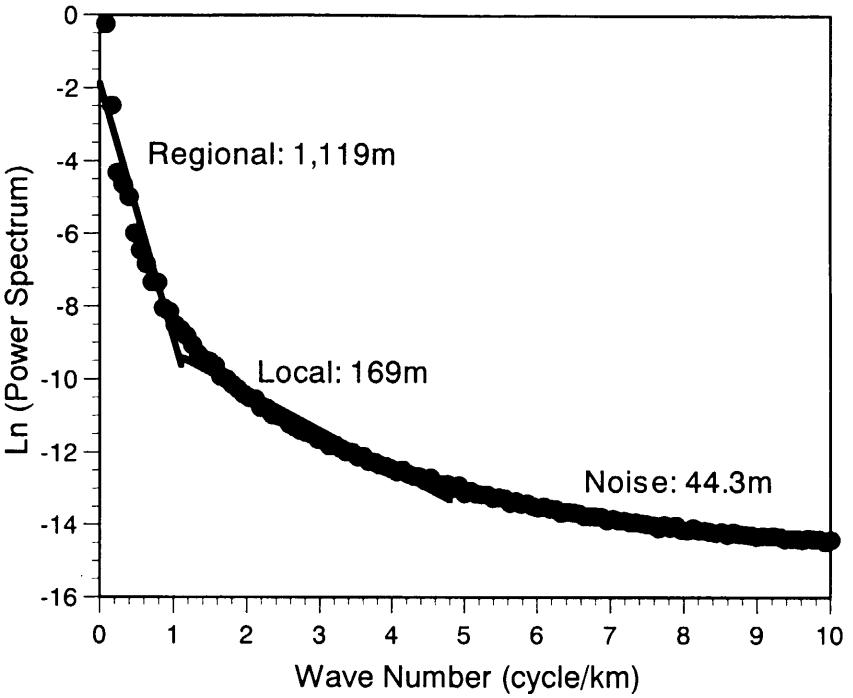

(a) Bazina Kebira prospect

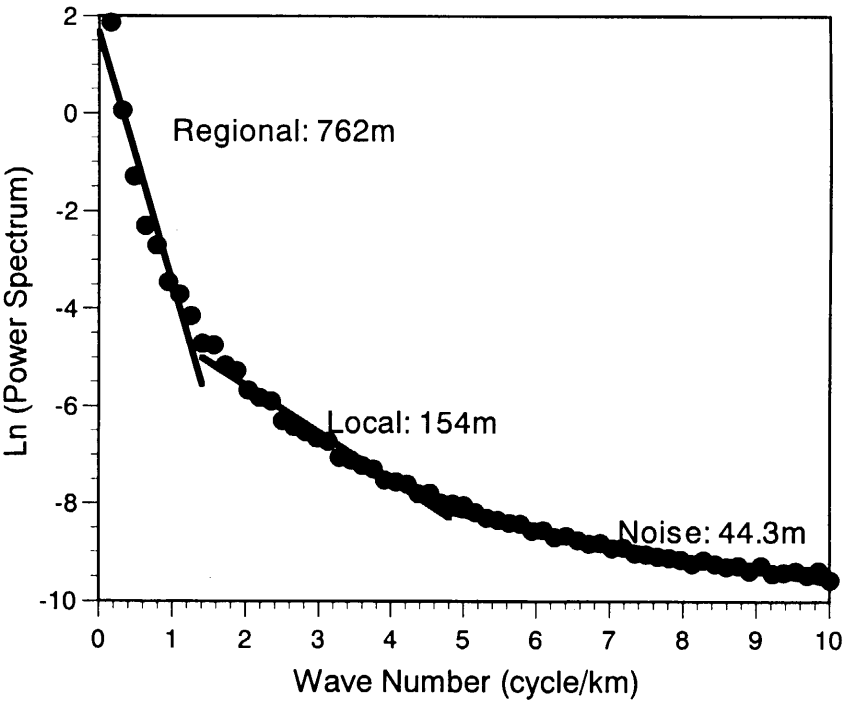

(b) Siliana prospect

Figure 14 Power Spectrum diagrams in every prospects

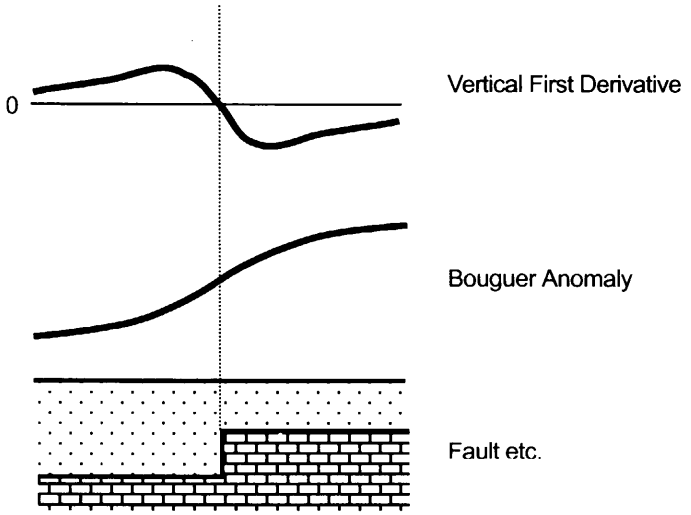

Figure 15 Enhancement of Vertical First Derivative Filter

which the number of measuring stations per unit area is one quarter of the current survey or less, is utilized as the trend surface for estimation of residuals. The result of residual estimation is illustrated in the residual gravity anomaly map.

A profile analysis along the 11 survey lines in the Bazina Kebira prospect and the 8 lines in the Siliana prospect is made so that the gravity residuals match with the subsurface density structures along these measuring lines. The best-fit models for given residuals are interactively approximated for its size and density structure, using the software for magnetic and gravity profile analysis, GM-SYS, developed by Northwest Geophysical Associates Co., Ltd. in USA. Then, the approximated best-fit models are further refined inversely by computing its size and density structure directly from the residuals. The standard gravity residuals are read on the residual gravity anomaly map. The densities for the subsurface models are expressed in their differences against the correction density for the each prospect.

1.2.3 IP survey

The flow chart of the current IP survey is shown in Figure 16.

The IP survey is carried out for the 11 measuring lines in the Bazina Kebira prospect and the 8 lines in the Siliana prospect according to the following specifications.

- Electrode Configureuration: Dipole-Dipole Array
- Electrode Spacing (a): 100 m
- Electrode Separation Index (n): 1 to 5

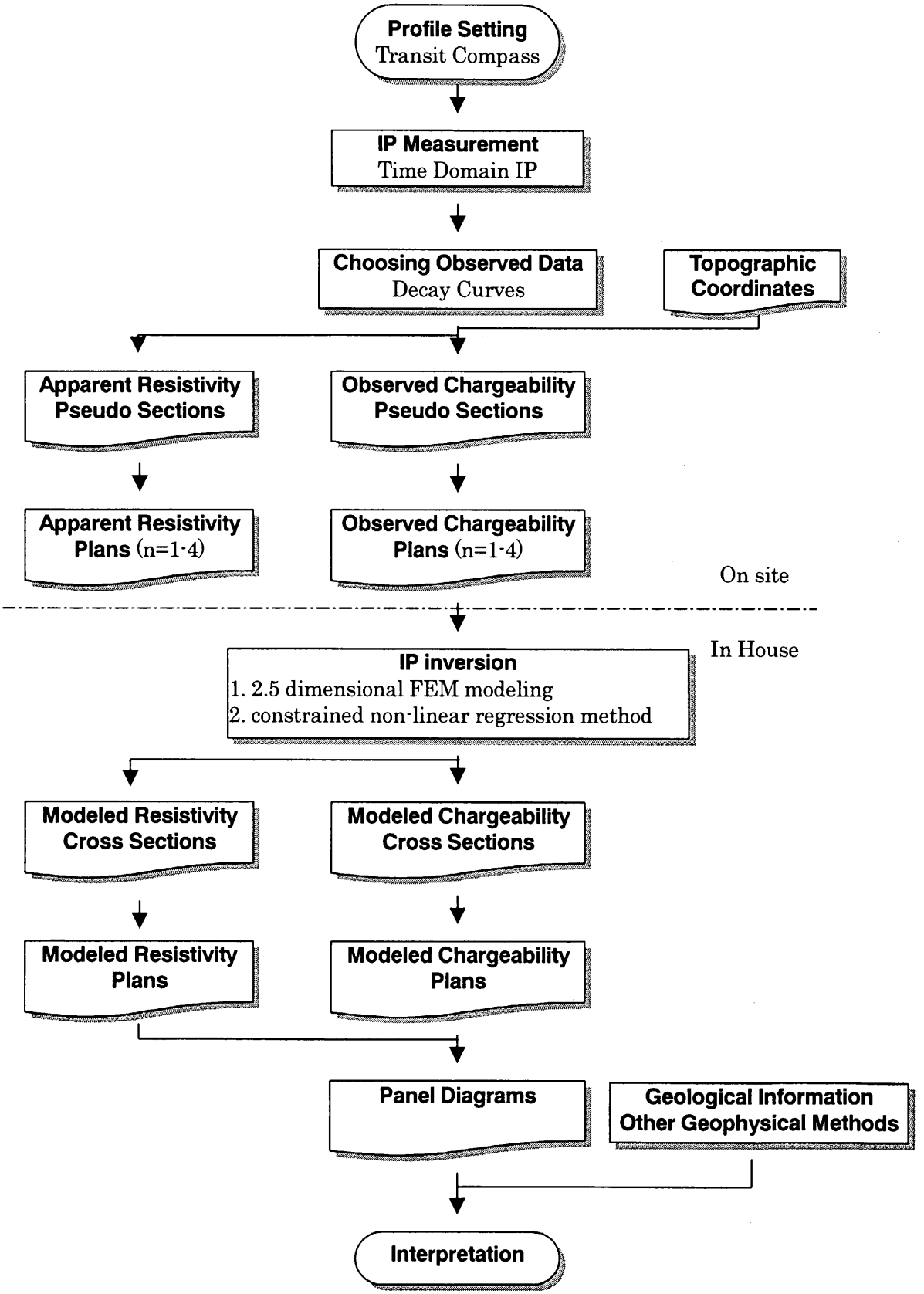

Figure 16 Flow chart of IP survey

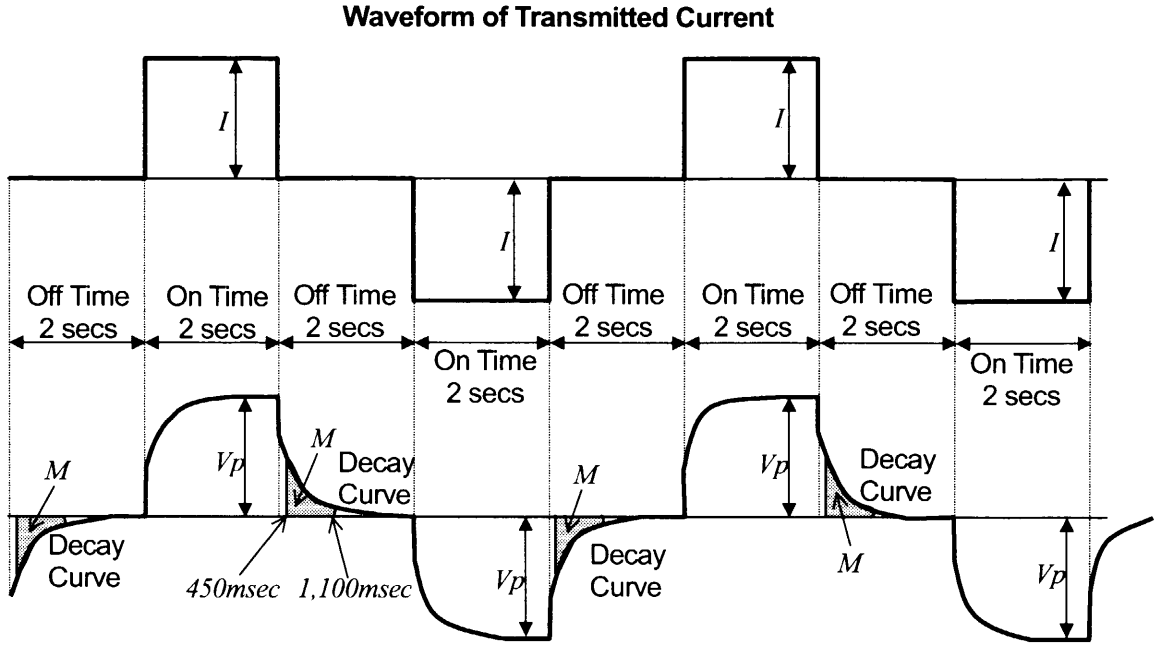

Figure 17 Schematic diagram of time domain IP

- Transmitted Current: Frequency = 0.125 Hz, Square-Wave with 50 % Duty Cycle
- IP Method: Time Domain
- Equipment Generator: Honda (Japan), Model ET4500 (Max. Output = 4.5 kVA, 3-Phase Alternate, 200 V)
  Transmitter: Phoenix (Canada), Model IPT-3 (Max. Output = 800 V −3.5 kVA)
  Receiver: Scintrex (Canada), Model PR-12(Accuracy = 1 μV)

The transmitting dipole, C1-C2, is stationed, while each of the 5 receiving dipoles, P1-P2, P2-P3, P3-P4, P4-P5 and P5-P6 is disposed at a pair of measuring stations in the opposite side. The measurement is made simultaneously at these receiving dipoles. Variation in voltage received at each dipole is shown in Figure 17. Apparent resistivity ρa (Ωm) is estimated, according to the equation (8), for the primary voltage V_p(V) that is the voltage stabilized at a certain level after current I(A) is transmitted.

$$\rho a = K\, Vp / I \tag{8}$$

where K is electrode configurration factor which is estimated for the dipole-dipole array used in the current survey according to the equation (9).

$$K = n(n-1)(n-2)\pi a \tag{9}$$

a: electrode spacing(m), n: electrode separation index

Chargeability M(mV/V or o/oo) is estimated, according to the equation (10), for the secondary voltage $V_s(t)$(unit: mV) that is a decayed voltage measured at a certain elapsed time after current shut-off. The integration range (t1=450msec–t2=1100msec) for chargeability estimation corresponds to that of the Newmont standard which is normally used in the time domain IP method.

$$M = \frac{1}{Vp\,(t1-t2)}\int_{t1}^{t2} Vs(t)\,dt \qquad (10)$$

More than 10 waveforms are collected at one measurement and compared to each other, in order to upgrade S/N (signal/noise) ratio. Although considerable current, averaging 0.3 A, is applied, observed V_p seldom exceeds 1mV due to extremely low ground resistivity. Where V_p is low as is the case, reproducible data can be obtained for apparent resistivity. However, it is very difficult to obtain smooth voltage decay curves. Measurements are repeated two to three times at one measuring station in order to obtain voltage decay curves with acceptable smoothness. Measurements along the survey lines in the NE-SW directions are disturbed by stronger noise than the lines in the NW-SE.

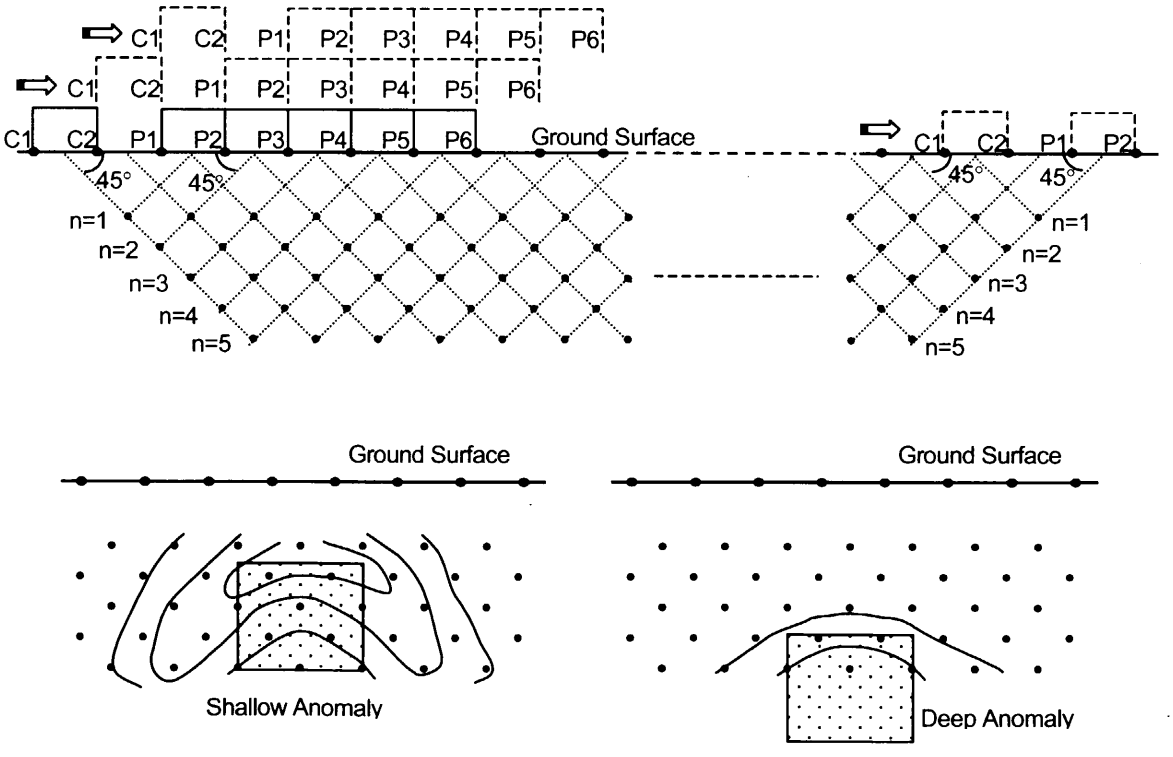

Figure 18 Plotting IP pseudo section with Dipole-Dipole Configuration and Typical Anomaly Pattern

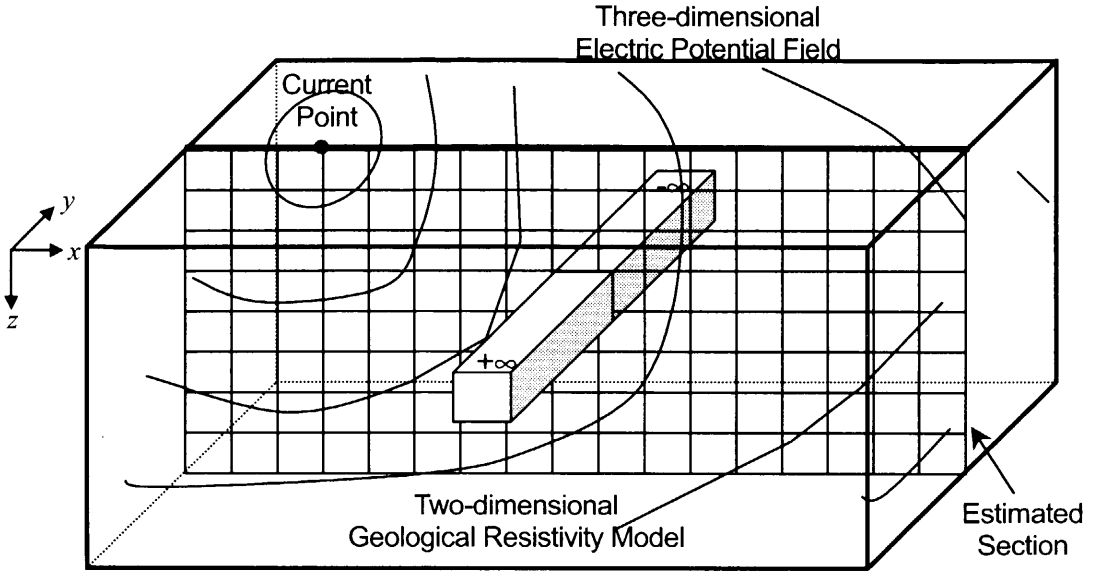

Figure 19 Schematic diagram of 2.5-D resistivity modeling

The measured apparent resistivity and chargeability are presented in pseudo-cross sections of apparent resistivity and chargeability for each survey line according to the plotting procedure illustrated in Figure 18. Based on these pseudo-cross sections, apparent resistivity and chargeability contour maps for the electrode separation indices, n =1,2,3 and 4, are prepared. An anomaly on a pseudo-cross section does not indicate actual geometry of a causative body as shown in Figure 18. It is, therefore, necessary to interpret the anomaly by 2-dimensional modeling analysis for geometry of a causative body on the relevant cross section. In the current investigation, field data are interpreted by combination of the 2.5 dimensional FEM (Finite Element Method) modeling and inversion using the constrained non-linear regression method as proposed by Sasaki (1992). The 2.5 dimensional FEM modeling proposed by Coggon (1977) assumes a prismatic model perpendicular to a cross section extending for a infinitive distance and estimates 3-dimensional voltage distribution applying the Fourier transformation over the assumed prismatic model in accordance with actually transmitted current. This modeling method, combined with inversion, has been put into practical use by Pelton, et al. (1978). Since inversion of apparent resistivity often becomes ill conditioned, the constraint, called 'Laplacean', is stipulated for its application in order to obtain stable solutions (Dey, et al., 1979). Therefore, the result of inversion is reliable for distribution of apparent resistivity, however, may not necessarily provide absolute values of apparent resistivity or chargeability. Figure 20 indicates elements of FEM used in the cross section analysis and an example of a block interpreted by inversion. A flow of inversion is

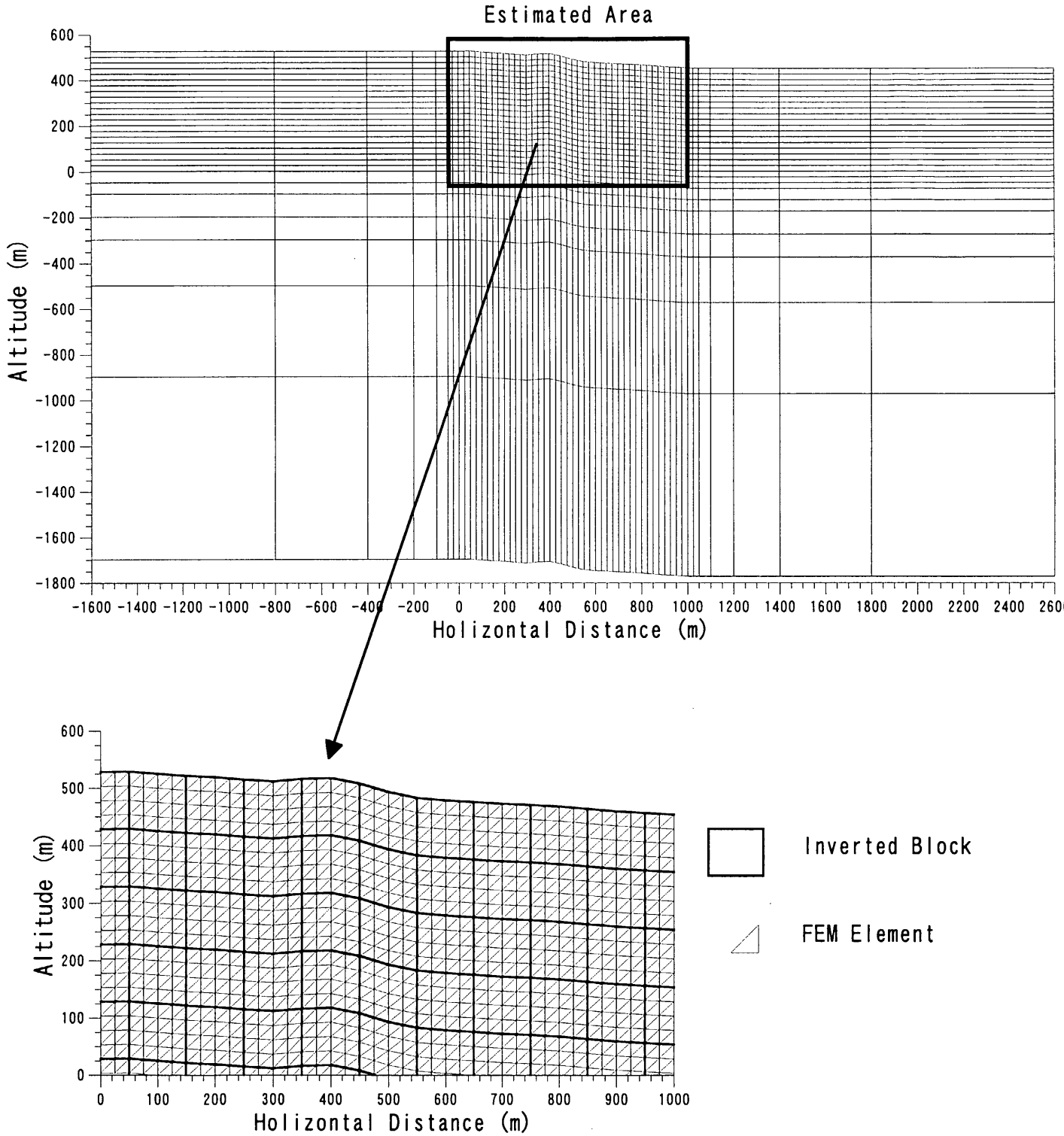

Figure 20 Mesh of 2.5-D Finite Element Method and Inverted Block

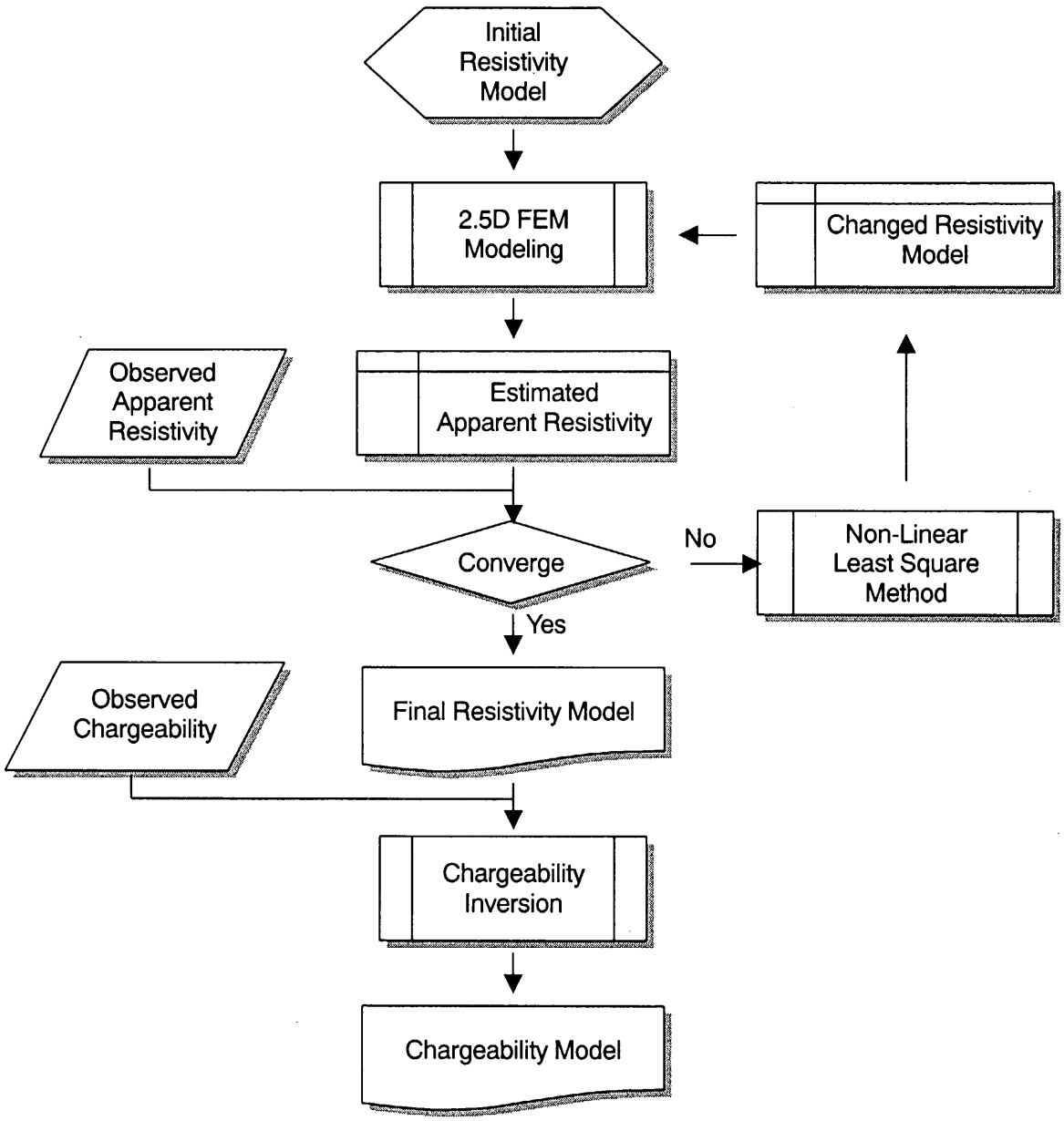

Figure 21 Flow chart of IP data inversion

shown in Figure 21. Interpreted apparent resistivity and chargeability are plotted on cross sections of measuring lines and are illustrated with contours. Contour plans of interpreted apparent resistivity and chargeability for elevations at specified levels above mean sea level are shown.

1.2.4 Laboratory Test

Density, resistivity and chargeability are measured in laboratory for 49 samples collected from outcrops, boreholes and mines within and around the prospect and shaped into prisms with a width of 4 cm and a length of 8 cm, or cylinders with a diameter of 3.5 cm.

Weights of samples are measured in atmosphere and water under 1) natural condition, 2) enforced wet condition, after immersed in tap water for more than 48 hours, and 3) enforced dry condition, after dried in a dry oven for more than 48 hours. Density is estimated using the equations, from (11) through (13). The result is collectively shown in Table 7.

$$\gamma n = W1/(W2-W3) \quad (11)$$

$$\gamma w = W2/(W2-W3) \quad (12)$$

$$\gamma d = W4/(W2-W3) \quad (13)$$

Where,

γn: natural dry density, γw: enforced wet density, γd: enforced dry density

$W1$: weight in atmosphere under natural condition

$W2$: weight in atmosphere under enforced wet condition

$W3$: weight in water under enforced wet condition

$W4$: weight in atmosphere under enforced dry condition

Resistivity ρ and chargeability M are measured using the field equipment of IPR 12 for samples held in GS type sample holders under enforced wet condition. The measurement device is illustrated in Figure 22. The equation (14) is used for estimation of resistivity, while readings of the receiver are converted to chargeability using the equation (10), the same as for the field measurement.

$$\rho = (S/l)(V/I) \quad (14)$$

Where, S: cross section area of sample, l: length of sample

V: received voltage (unit: V), I: transmitted current (unit: A)

The result of resistivity measurement is shown in Table 8. Table 9 shows the result of conductivity mesurement of river water, well water and tap water in and around the prospects by using a handy conductivity meter manufactured by the TOA electric wave Co., Ltd. In consideration of the estimated average conductivity of 3,840μS/cm, a NaCl solution of

Table 7 Results of rock density measurement of specimens

No.	Location	Geology	Rock	Weight (g)				Density (g/cm^3)			Porosity (%)
				W1	W2	W3	W4	Natural	Wet	Dry	
1	A4-30	Transition Zone	Mineralized Limestone	138.92	140.01	102.54	138.13	3.707	3.737	3.686	5.02
2	A4-30	〃	〃	155.04	155.29	113.53	154.37	3.713	3.719	3.697	2.20
3	A4-30	Triassic	Gypsum	113.68	113.91	75.14	100.67	2.932	2.938	2.597	34.15
4	A0-320	Cretaceous (Aptian)	Mineralized Vein	119.47	122.61	89.61	118.38	3.620	3.715	3.587	12.82
5	A6-125	Quaternary (Pliocen)	Polygenetic Breccia	119.94	122.11	74.05	119.07	2.496	2.541	2.478	6.33
6	A0-370	Cretaceous (Aptian)	Weak Argillic Limestone	96.32	96.76	60.71	95.68	2.672	2.684	2.654	3.00
7	A6-170	Cretaceous	〃	70.29	71.07	44.22	69.70	2.618	2.647	2.596	5.10
8	A1-135	Cretaceous (Upper)	Massive Limestone	89.70	90.36	56.42	89.36	2.643	2.662	2.633	2.95
9	A1-125	Quaternary (Eocene)	Limestone	154.78	157.38	96.80	153.59	2.555	2.598	2.535	6.26
10	A1-50	〃	〃	169.34	170.39	106.05	169.00	2.632	2.648	2.627	2.16
11	A2-130	〃	〃	125.29	125.78	78.80	125.16	2.667	2.677	2.664	1.32
12	A3-180	Cretaceous (Lower)	Argillic Limestone	47.33	47.73	29.75	47.11	2.632	2.655	2.620	3.45
13	A3-85	Triassic	Dolomite	174.17	174.70	112.73	174.03	2.811	2.819	2.808	1.08
14	A3-80	〃	Psammite	128.39	133.80	74.86	124.73	2.178	2.270	2.116	15.39
15	A5-50	Cretaceous (Upper)	Limestone	49.04	51.06	30.55	48.77	2.391	2.490	2.378	11.17
16	A6-50	Quaternary (Miocene)	Breccia Sandstone	105.37	106.08	66.14	104.79	2.638	2.656	2.624	3.23
17	A2-140	Triassic	Mica Sandstone	65.00	68.17	39.10	64.58	2.236	2.345	2.222	12.35
18	A4-190	Quaternary (Pliocen)	Limestone Conglomerate	141.61	143.02	88.21	140.90	2.584	2.609	2.571	3.87
19	A3-140	Quaternary	〃	42.28	47.40	25.48	41.40	1.929	2.162	1.889	27.37
20	C0-500	Triassic	Gypsum	79.87	82.20	39.01	61.11	1.849	1.903	1.415	48.83
21	L3-90	Transition Zone	Mineralized Breccia	161.91	168.49	100.43	160.46	2.379	2.476	2.358	11.80
22	C10-80	Cretaceous (Aptian)	Mineralized Sandstone	163.80	165.63	103.26	162.66	2.626	2.656	2.608	4.76
23	C10-80	〃	〃	172.36	176.83	109.41	171.35	2.557	2.623	2.542	8.13
24	C10-80	〃	〃	76.50	80.81	46.74	75.61	2.245	2.372	2.219	15.26
25	C10-80	〃	〃	74.65	75.48	47.64	74.19	2.681	2.711	2.665	4.63

Table 7 Results of rock density measurement of specimens (continued)

No.	Location	Geology	Rock	Weight (g)				Density (g/cm^3)			Porosity (%)
				W1	W2	W3	W4	Natural	Wet	Dry	
26	C10-80	〃	〃	186.60	188.86	119.29	185.59	2.682	2.715	2.668	4.70
27	C10-80	〃	〃	151.20	151.99	94.50	150.86	2.630	2.644	2.624	1.97
28	C10-80	〃	〃	140.14	142.29	86.65	139.37	2.519	2.557	2.505	5.25
29	C10-20	Triassic	Carbonated Sandstone	123.13	128.21	74.05	121.66	2.273	2.367	2.246	12.09
30	C12-10	Quaternary	Consolidated Sand	346.15	347.07	223.89	345.86	2.810	2.818	2.808	0.98
31	C0-700	〃	〃	345.54	353.44	223.40	344.84	2.657	2.718	2.652	6.61
32	C15-40	〃	〃	398.83	399.81	267.07	397.65	3.005	3.012	2.996	1.63
33	C0-760	〃	〃	323.89	325.35	202.94	323.25	2.646	2.658	2.641	1.72
34	C0-760	Transition Zone	Sandstone	316.32	325.40	199.74	314.25	2.517	2.590	2.501	8.87
35	C0-760	〃	〃	446.86	452.40	324.05	445.00	3.482	3.525	3.467	5.77
36	C0-760	Cretaceous	Limestone Breccia	345.36	348.87	217.44	344.03	2.628	2.654	2.618	3.68
37	C0-760	Transition Zone	〃	275.85	296.74	174.01	273.50	2.248	2.418	2.228	18.94
38	FD-1	〃	Limestone Dolomite	380.84	381.66	248.86	380.06	2.868	2.874	2.862	1.20
39	FD-2	〃	〃	431.28	438.45	314.11	430.07	3.469	3.526	3.459	6.74
40	MJTK-L2 380m	Cretaceous	Mineralized Limestone Vein	241.54	242.73	167.64	241.37	3.217	3.233	3.214	1.81
41	MJTK-L2 381m	〃	Mineralized Limestone	488.13	488.90	380.42	487.91	4.500	4.507	4.498	0.91
42	MJTK-L2 270m	〃	Mineralized Argillic Limestone	252.45	257.69	169.44	252.15	2.861	2.920	2.857	6.28
43	MJTK-L1 111m	Triassic	Maar	465.51	483.17	269.68	410.06	2.180	2.263	1.921	34.25
44	MJTK-L1 92m	〃	〃	313.15	344.04	179.09	274.41	1.898	2.086	1.664	42.21
45	C1-60	〃	Limestone	327.80	338.59	207.57	327.35	2.502	2.584	2.498	8.58
46	C2-0	〃	Dolomite	377.51	377.79	245.84	377.21	2.861	2.863	2.859	0.44
47	C7-35	〃	〃	377.36	380.91	244.89	377.08	2.774	2.800	2.772	2.82
48	C7-115	Quaternary	Massive Sandstone	351.11	356.60	223.78	349.82	2.644	2.685	2.634	5.10
49	C0-420	Triassic	Psammite	354.43	360.17	215.89	354.16	2.457	2.496	2.455	4.17

Table 8 Results of IP measurement of specimens

No.	Location	Geology	Rock	Section (cm^2)	Length (cm)	Current (μA)	Voltage (mV)	Resistivity (Ωm)	Chargeability (mV/V)
1	A4-30	Transition Zone	Mineralized Limestone	6.67	5.70	100	267.04	31.3	130.19
2	A4-30	〃	〃	6.67	6.32	5	1511.26	3191.7	3.16
3	A4-30	Triassic	Gypsum	6.67	5.73	100	416.31	48.5	34.61
4	A0-320	Cretaceous (Aptian)	Mineralized Vein	6.67	4.98	100	4576.30	613.9	8.60
5	A6-125	Quaternary (Pliocen)	Polygenetic Breccia	6.70	7.24	50	3361.23	622.2	9.92
6	A0-370	Cretaceous (Aptian)	Weak Argillic Limestone	6.69	5.41	80	3527.76	545.1	1.57
7	A6-170	Cretaceous	〃	6.67	4.14	100	2775.65	447.4	8.49
8	A1-135	Cretaceous (Upper)	Massive Limestone	6.68	5.10	90	3403.49	495.5	1.14
9	A1-125	Quaternary (Eocene)	Limestone	9.36	6.53	100	945.33	135.6	2.81
10	A1-50	〃	〃	9.36	6.90	10	2484.10	3371.3	9.90
11	A2-130	〃	〃	9.38	5.04	5	2188.63	8142.5	6.64
12	A3-180	Cretaceous (Lower)	Argillic Limestone	6.67	2.70	50	668.86	330.6	1.30
13	A3-85	Triassic	Dolomite	9.38	6.65	5	2237.55	6313.8	0.70
14	A3-80	〃	Psammite	9.36	6.35	100	782.47	115.4	2.55
15	A5-50	Cretaceous (Upper)	Limestone	6.67	3.09	100	499.59	107.9	0.93
16	A6-50	Quaternary (Miocene)	Breccia Sandstone	6.67	6.08	100	2363.95	259.5	7.81
17	A2-140	Triassic	Mica Sandstone	4.70	6.27	100	1100.26	82.4	6.74
18	A4-190	Quaternary (Pliocen)	Limestone Conglomerate	9.36	5.90	100	2853.35	452.6	8.20
19	A3-140	Quaternary	〃	4.67	4.76	100	475.41	46.7	2.95
20	C0-500	Triassic	Gypsum	9.35	4.72	-	-	-	-
21	L3-90	Transition Zone	Mineralized Breccia	9.36	7.30	100	1823.23	233.9	1.28
22	C10-80	Cretaceous (Aptian)	Mineralized Sandstone	9.36	6.70	100	2666.71	372.5	3.18
23	C10-80	〃	〃	9.37	7.17	100	1178.63	154.0	42.01
24	C10-80	〃	〃	6.63	5.17	100	549.52	70.5	0.36
25	C10-80	〃	〃	6.66	4.23	100	1715.62	270.3	59.63

Table 8 Results of IP measurement of specimens (continued)

No.	Location	Geology	Rock	Section (cm^2)	Length (cm)	Current (μA)	Voltage (mV)	Resistivity (Ωm)	Chargeability (mV/V)
26	C10-80	〃	〃	9.36	7.47	100	552.19	69.3	141.25
27	C10-80	〃	〃	9.38	6.17	30	2389.62	1210.3	6.96
28	C10-80	〃	〃	9.38	5.99	100	1754.55	274.8	1.43
29	C10-20	Triassic	Carbonated Sandstone	9.36	5.83	100	2352.47	377.9	3.25
30	C12-10	Quaternary	Consolidated Sand	17.15	8.15	3	1046.70	7341.9	0.65
31	C0-700	〃	〃	16.25	8.12	100	3808.20	761.9	3.62
32	C15-40	〃	〃	16.49	8.22	100	158.67	31.8	96.58
33	C0-760	〃	〃	15.75	8.13	50	3291.15	1274.8	13.44
34	C0-760	Transition Zone	Sandstone	15.96	8.10	100	1321.53	260.4	7.09
35	C0-760	〃	〃	16.13	8.09	100	2107.84	420.3	8.91
36	C0-760	Cretaceous	Limestone Breccia	16.58	8.15	100	3495.55	711.1	13.59
37	C0-760	Transition Zone	〃	16.21	8.06	100	935.36	188.1	7.64
38	FD-1	〃	Limestone Dolomite	16.71	8.11	100	2111.43	435.0	35.05
39	FD-2	〃	〃	16.07	8.08	100	452.76	90.0	32.21
40	MJTK-L2 380m	Cretaceous	Mineralized Limestone Vein	8.90	9.00	10	1614.52	1596.6	13.41
41	MJTK-L2 381m	〃	Mineralized Limestone	8.90	12.55	100	444.64	31.5	116.54
42	MJTK-L2 270m	〃	Mineralized Argillic Limestone	8.90	11.20	100	3688.17	293.1	34.54
43	MJTK-L1 111m	Triassic	Maar	17.89	11.82	100	136.86	20.7	4.43
44	MJTK-L1 92m	〃	〃	17.72	9.30	100	99.98	19.1	2.85
45	C1-60	〃	Limestone	16.36	8.21	100	3015.43	600.7	2.08
46	C2-0	〃	Dolomite	16.50	8.17	3	2566.90	17280.2	1.50
47	C7-35	〃	〃	17.58	8.22	10	1022.92	2187.1	0.57
48	C7-115	Quaternary	Massive Sandstone	16.67	8.11	10	1723.67	3543.0	3.29
49	C0-420	Triassic	Psammite	18.17	8.08	100	3396.63	763.8	9.57

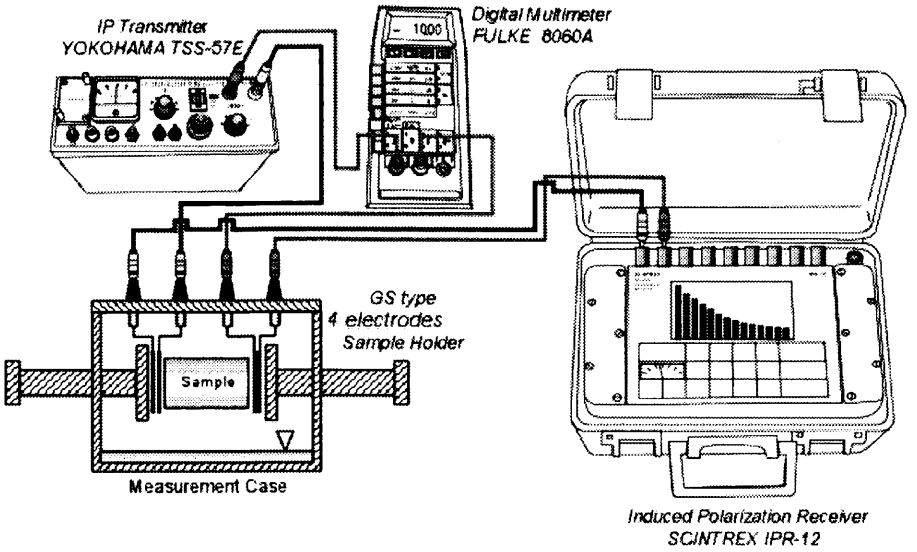

Figure 22 Schematic diagram of IP measurement for a rock sample

2,000 μS/cm conductive, equivalent to 5.0 Ωm, was produced for immersing the samples. The solution indicated conductivity of 2,031 μS/cm, at a temperature of 20.7 degrees Celsius at the time of measurement.

Table 9 Conductivity of Water Samples Acquired in or near the Survey Area

Sampling Point	Kind of Water	Temperature (℃)	Conductivity (mS/cm)	Resistivity (Ωm)
Farm near the Gâafour	Surface	22.4	4.740	2.110
Hotel in the Gâafour	Tap	23.5	1.130	8.850
Siliana river	River	22.0	6.450	1.550
Well between A6-20 and A7-20	Well	22.0	2.098	4.766
Siliana river near A7-65	River	22.8	9.740	1.027
Well near A0-70	Well	22.0	1.485	6.734
Stream between A2-50 and A2-45	River	20.5	1.950	5.128
Water Source near C5-100	Spring	21.5	3.310	3.021
Stream near C12-100	River	20.8	3.660	2.732

1.3 Result

1.3.1 Laboratory Test

Enforced wet densities of 49 rock samples collected in and around the prospects are resulted in the range between 1.81 through 3.68 g/cm^3 from density measurement in laboratory on Table 10. The estimated average density of 2.60 g/cm^3 is higher than the correction density of 2.3 and 2.4 g/cm^3 adopted in the current gravity survey. Around a half of samples are collected from mineral occurences sparsly distributed within the prospects. The average desity of 2.44

g/cm^3 within the other samples are roughly same as the correction density of the current gravity survey. Hard rock samples with better property are measoured in the many case of laboratory test, although many fragile rocks possibly disintegrated during shaping or immersion are lying in the field. Average density of rock samples decreases in order of the dolomitic rock of 2.66 g/cm^3 in the Triassic system, the Cretaceous and Tertiary system of 2.57 g/cm^3, the Quaternary system 2.40 g/cm^3 and the other rocks of 2.14 g/cm^3 in the Triassic system. The highest average density of 2.81 g/cm^3 is indicated in the rocks collected around the mineral occurences.

Table 10 Rock Properties Resulting from Laboratory Test

Geological Time	Rock	Sample	Density (g/cm^3)			Resistivity (Ωm)			Chargeability (mV/V)		
			Min.	Max.	Average	Min.	Max..	Average	Min.	Max.	Average
Quaternary	Sandstone, Sand	4	2.16	2.82	2.60	46.7	7,342	2,923	0.7	3.6	2.6
Tertiary	Limestone, conglomerate, Etc.	6	2.54	2.68	2.62	135.6	8,143	2,164	2.8	9.9	7.5
Cretacious	Limestone	5	2.49	2.68	2.63	107.9	545	385	0.9	8.5	2.7
Triassic	Dolomite	4	2.58	2.86	2.77	600.1	17,280	6,595	0.6	2.1	1.2
Triassic	Sandstone, Maar, Gypsum	7	1.90	2.50	2.25	19.1	764	230	2.6	9.6	4.9
Subtotal		26	1.90	2.86	2.54	19.1	17,280	2,175	0.6	9.9	4.1
Mineralized		23	2.11	4.51	2.99	31.3	3,192	516	0.4	141.3	35.3
Total		49	1.90	4.51	2.75	19.1	17,280	1,380	0.4	141.3	19.1

The results from resistivity and chargeability measurement of 48 rock samples measured density, except for a sample disintegrated during immersion, are shown in Table 9. Resistivities ranging from 19 to 17,280 Ωm are averaged around 1,500 Ωm. Rock resistivity ρr is affected by resistivity of pore water ρw and porosity ϕ, as represented following Archie's formula (Archie, 1941).

$$F=\rho r/\rho w=a\phi^{-m} \qquad (15)$$

Where, F is proportional factor called the formation resistivity factor, a called tortosity factor and m called cementing factor are experimentally estimated in every geological unit. Tortosity factor indicates value around one, cementing factor is ranging between 0.8 and 2.5. In the previous program, it was suggested that the relatively resistive water around 14 Ωm for immersing samples makes the measured resistivity of rocks in laboratory higher than in field. In the current program, it is guessed that the water resistivity around 14 Ωm decided in consideration with the result of conductivity measurements in field decreases the diffrence between of results between in field survey and in laboratory test. The result of the laboratory

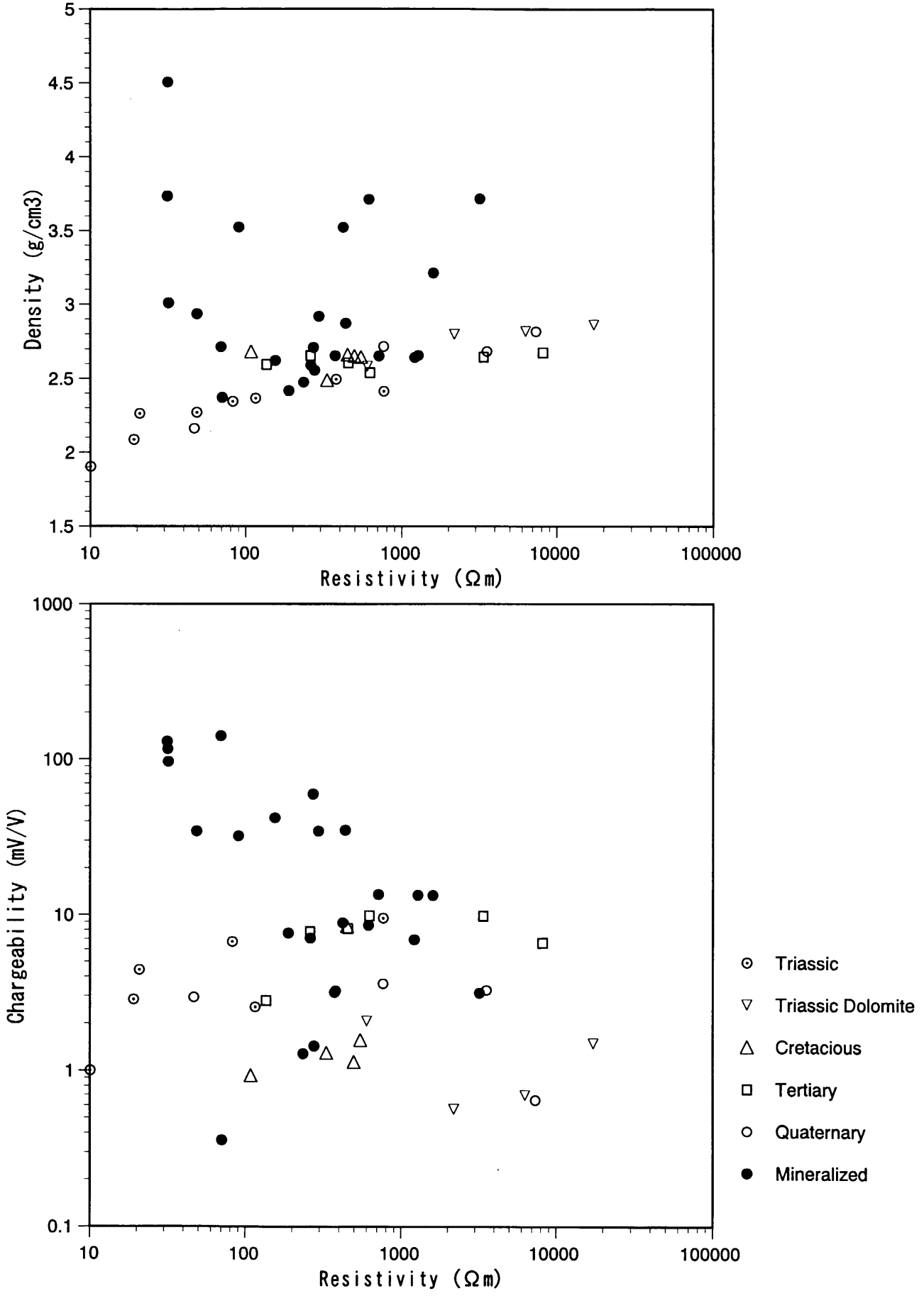

Figure 23 Cross plots of Density and Chargeability for resistivity of rock specimens

test appears the average resisitivity of the Quaternary and Tertiary systems higher than that of the older systems. However, it is recommended that the general resistivity of them can't be estimated from only the result of laboratory test because soft rocks and soils are distributed widely the area of the Quaternary and Tertiary systems. Though the limestone samples of the Cretaceous system indicated higher resistivity more than 1,000 Ωm in the previous test, they decrease to several hundreds Ωm in the current test. The measurement resistivity in the field and the density resulted in the laboratory indicate similar results. The fact suggests the property of limestones in the current prospect is different from that in the Bou Khil prospect and the El Akouat prospect. In the Triassic system, the dolomites indicate high density and high resistivity, while the other rocks show conductive. Though many mineralized samples appear conductive, the resistivity of mineralized rock is distributed in the range between 31 througt 3,192 Ωm too widely to classify their mineralizaion.

It is difficult to estimate geological unit according to the chargeability of samples. The chargeablity of mineralized samples is distigushed clearly from that of the others. The chargeability of the non-minaralized samples is ratively low ranging between 0.6 and 9.9 mV/V, while the 13 mineralized samples indicate high chargeablity more than 10 mV/V and the average chargeability of all 23 mineralized samples is estimated around 35mV/V. There are 3 mineralized samples indicating extremely high chargeability beyond 100 mV/V. The network type and the vein type of mineralization tend to become higher chargeability than the dissimination type. It is convinced that the chargeability of samples including much galena and pylite indicates higher than that of the samples including much sphalerite.

The cross plots on measured density, resistivity and chargeability of samples are shown in Figure 23. Resistive rocks of the non-mineralized samples tend to increase density, but their correlation is weak and no valid correlation between resistivity and density of the mineralized samples. There is no valid correlation between resistivity and chargeability of the non-mineralized samples, while weak correlation is indiced within the mineralized samples. The fact leads their metal factor represented the ratio of chargeability for resistivity effective.

1.3.2 Bazina Kebira Prospect

(1) Geology

The summary geological plan of the Bazina Kebira prospect is shown in Figure 11 respectively. The stratigraphy comprises Triassic, Cretaceous and Tertiary systems overlain by Quaternary system.

Lambert X (m)

445000 445500 446000 446500 447000 447500 448000 448500 449000 449500 450000 450500 451000 451500 452000 452500 453000 453500 454000 454500 455000 455500 456000

Lambert Y (m)

345500 345000 344500 344000 343500 343000 342500 342000 341500 341000 340500 340000 339500 339000 338500 338000

Koudiat Safra Mine

Koudiat Soda Mine

Kodiat Tiliett

H'Zamel Assoued

Bazaina Kebira

C1 C2 C3 C4 C5 C6 C7 C8 C9 C10 C11 C12 C13 C14 C15 C16 C17 C18 C20

GEOLOGY

Quaternary

Holocene — Q, Qc

Pleistocene — eQ

Tertiary

Pliocene — Mt

Miocene - Pliocene — M-P

Oligocene — O

Eocene - Paleocene — Ep-e

Cretaceous

Maastrichtian — Cma

Campanian - Maastrichtian — Cca-ma

Campanian — Cca

Coniacian - Campanian — Cco-ca

Cenemonian - Turonian — Cce-tu

Albian - Cenemonian — Cal-ce

Barremian - Aptian — Cba-ap

Triassic

Td, Tc, Tb, Ta

Fault

0 500 1000 1500 2000

Figure 24

Geological Map
in Bazina Kebira Prospect

Scale 1 : 30,000

March, 2001

The Triassic system distributes in the northern to western part of the prospect and is unconformably overlain by the Oligocene series in its center. The system is the northeastern part of the Jebel Ech Cheid diapir comprising rock salt in its core, gypsum, dolomite, slate, limestone and other minor rock types. Its weathered outcrops show brown to dark brown colors due to oxidation of Fe and Mn bearing minerals contained in the dolomite in minor amount. The limestone, yellowish to dark gray and massive, is generally recrystallized and seldom contains poorly preserved fossils.

The Cretaceous system is divided into Barremian-Aptian, Albian-Cenomanian, Cenomanian-Turonian, Coniacian-Campanian and Upper Campanian-Maastrichtian formations in stratigraphically ascending order. The Barremian-Aptian formation distributes in the northwestern part, from Koudiat Safra to H' Zamel Assoued, and is fault-contacted with the Triassic system. Its lower member consists of alternation of gray limestone and green slate, while the upper member is essentially composed of grayish white limestone. Beddings generally strike in the NE-SW direction and dip to the northwest. The Albian-Cenomanian formation distributes in the vicinity of H'Zamel Assoued in the northwestern part and is fault-contacted with the Barremian-Aptian formation. The formation comprises green marl and argillaceous limestone. The Cenomanian-Turonian formation, distributing in the central part to the northeast of Koudiat Safra and Koudiat Soda, is fault-contacted with the Triassic system and is conformably overlain by the Coniacian-Campanian series. The formation is divided into the lower, middle and upper members. The lower member consists of gray tabular limestone, the middle member, of alternation of bluish gray marl and limestone, and the upper member, of gray tabular limestone. Beddings generally strike in the NW-SE direction and dip to the northeast. The Coniacian-Campanian formation, conformably overlying the Cenomanian-Turonian formation, distributes in the vicinity of Koudiat Safra in the central part and mainly comprises gray marl and gray, argillaceous limestone. Beddings generally strike in the NE-SW direction and dip to the northwest. The Upper Campanian-Maastrichtian formation, mainly comprising gray limestone, distributes in the vicinity of Koudiat Tlilette and Koudiat Soda in the central part and is fault-contacted with the Triassic system. Although beddings generally strike in the NE-SW direction and dip to the northwest, they show somewhat complex attitudes in the vicinity of Koudiat Tlilette where a minor anticline is located.

The Tertiary system, in the northwestern, southwestern through eastern part of the prospect, is divided into Paleo-Eocene, Oligocene and Mio-Pliocene series. The Paleo-Eocene series, distributing around Koudiat Soda in the central part, conformably overlies the Upper

Campanian-Maastrichtian formation at around Koudiat Soda, while it covers directly the Campanian formation with unconformity to the northeast of Koudiat Soda. The series mainly consists of black marl, containing gypsum and fragments of organic remains. Index fossils yielded from the upper part of this series indicate the Lutetian stage of Eocene. Beddings strike in the E-W direction and dip to the north in general. The Oligocene series, unconformably overlying the stratigraphically lower formations, distributes from Koudiat Tlilette to Koudiat Soda in the northwestern to eastern part. This series consists of reddish brown sandstone containing fragments of organic remains, and is seldom interbedded with layers of marl and conglomerate. Beddings strike in the NE-SW to E-W direction and dip to the north or northwest. The Mio-Pliocene series distributes in the eastern part and mainly comprises sandstone, interbedded with lenses of green marl and red slate.

The Quaternary system comprises talus, colluvial and alluvial deposits. Talus and colluvial deposits distribute in hills and foot-hills and consist of gravel, sand and clay. Alluvial deposits are developed in plains along rivers and water courses and consist of gravel, sand and clay.

The major structural elements that are observed in the Triassic to Tertiary systems in the prospect are diapirs and fault systems trending in the N-S, NE-SW and ENE-WSW directions.

A topographic high, elongated in the NE-SW direction, is located in the northwestern part of the general area including the prospect. This characteristic morphology is an expression of an anticline or dome formed by intrusion of a diapir consisting of the Triassic system. The topographic high has its peak in the vicinity of Jebel Ech Cheid, thus called 'Jebel Ech Cheid diapir', and slopes away towards northwest and southeast.

The Triassic system is in contact with the Cretaceous and Tertiary systems to the southeast bounded by a fault or unconformity. A number of north-south running faults can be assumed to the northeast of Koudiat Safra, where alignments of dolomite and limestone strata are laterally offset step-by-step in the north-south direction. Strata of the Cretaceous and Tertiary systems indicate a homoclinal structure, striking in the NE-SW direction and dipping 25 to 70° to the northwest in general. To the southeastern side of the diapir, however, overturn folds are extensively developed due to diapirism. A particularly complex structural zone runs from Koudiat Safra to Koudiat Tlilett with its width of about 250 m, and continues to an area where a number of north-south trending faults make the structure further complex.

Faults are categorized into the N-S trending and the NE-SW or ENE-WSW trending systems, with the former crosscutting the latter. The fault systems break up the Cretaceous

and the Paleogene systems into a number of blocks, each of which indicates its own geologic characteristics. In addition, a number of small scale folds are commonly formed by intrusion of the diapir.

(2) Gravity survey

Characteristics of Bouguer anomaly (hereinafter called 'gravity') distribution are described below.

①Regional Gravity Distribution (Figures 10 and 11)

The NE-SW and crosscutting NW-SW gravity trends are predominated in the region including the Bazina Kebira prospect, reflecting the regional geological structure, according to the regional gravity distribution (Figure 10) as the result of the project carried out by the ONM. The known ore deposits of The Bou K'hil and the El Akhouat prospects investigated in the previous program and the Fejera Doume working mine are located in and around gravity high. Though diapirs tend to be related to gravity high, a diapir is generated by rise of a low density rock mass upwards. The fact suggests that diapirs don't indicate high gravity, but other geological structures related to diapirs such as anticline increase gravity.

The Bazina Kebira prospect is located in the southeastern side of the narrow area of gravity high, which is outlined by the 0 meal contour and stretches northeastward along the Djebel Ech Chied hills. Three high gravity anomalies lies within the narrow gravity high, the prospect is located around the center and northeastern anomalies of them. Two extensive gravity low areas which trend in the NW-SE direction lie in the El Aroussa plain and the Teboursouk plain, which spread in the both sides of the Djebel Ech Chied hills. The prospect is laid in the marginal zone of steep gravity gradient from the narrow gravity high southeastward the gravity low in the El Aroussa plain.

②Gravity Distribution of the Prospect (Figure 25)

The gravity distribution of the prospect is divided into the southwestern and northeastern parts from the Koudiat Safra ore deposit of the old Sidi Ayed mine.

In the northeastern part, the zone of steep gravity gradient from the narrow gravity high runs between the extensive gravity high beyond -4 mgal, centering in the vicinity of the Lambert coordination of 449500E and 345000N in the northwest side, and the extensive gravity low below -17 mgal, centering in the vicinity of the Lambert coordination of 455500E and 343000N in the southeast side. The Koudiat Soda ore deposit is located in the southeastern margin of this steep gravity gradient zone.

In the southwestern part, gravity decreases southeastwards from –5 to –10 mgal. The range in this part is not so broad as in the northeastern part, and the contour intervals are

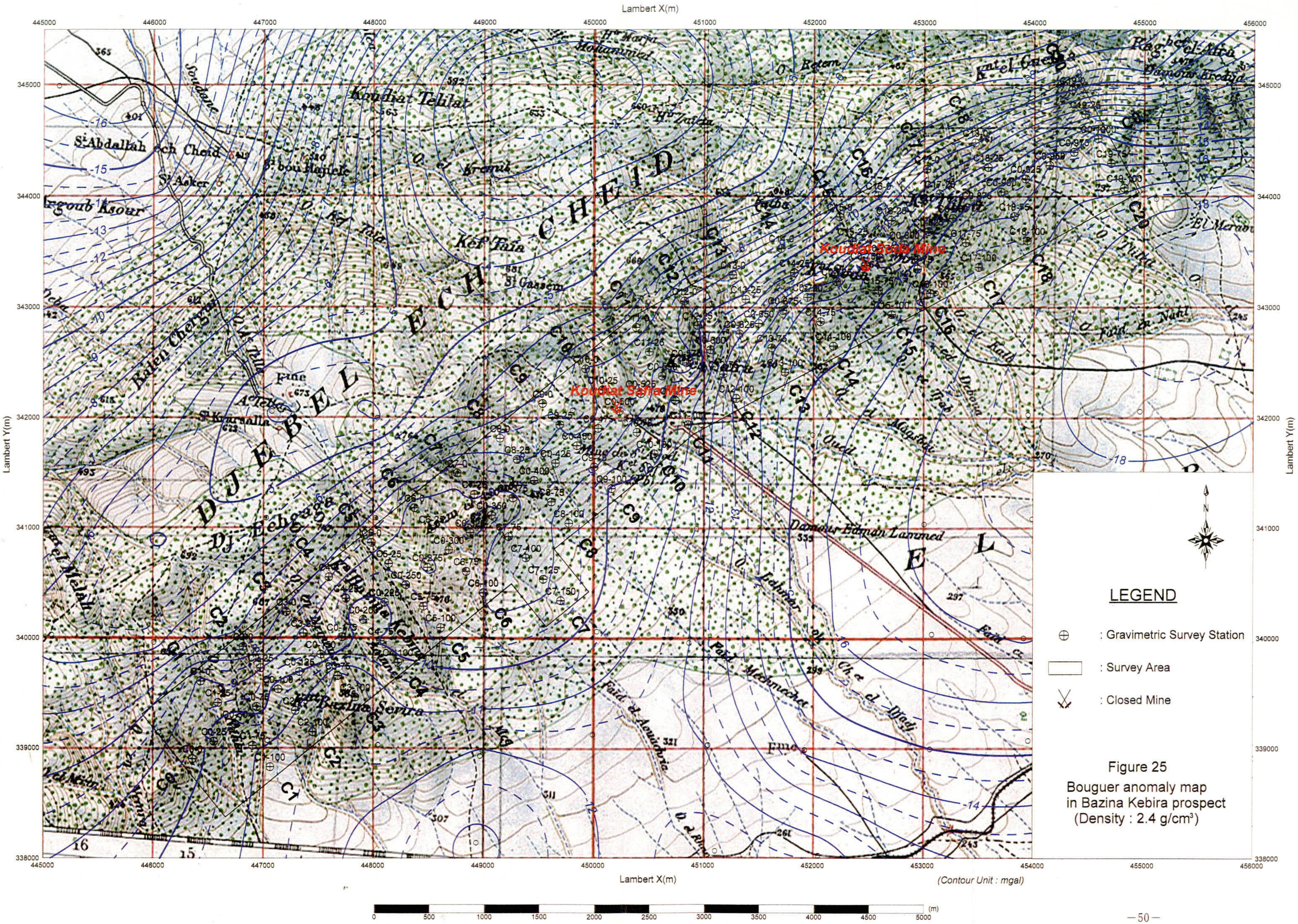

Figure 25
Bouguer anomaly map
in Bazina Kebira prospect
(Density : 2.4 g/cm³)

relatively long. This part is characterized by the overhung around the survey line C7. The gravity in the area between the line C5 and C8 is almost invariable. The overhung continues on a saddle of a gravity high dividing the extensive gravity low in the El Arrousa plain. The H'Zamel Assoued mineral occurrence is located on the overhung of the gravity high.

③Residual Gravity Anomaly (Figure 26)

Residual gravity low extends within the almost prospect except for small gravity high anomalies beyond 0 mgal in the vicinity of the Koudiat Safra ore deposit in the central part and in the southeastern side of the line C7 in the southwestern part.

In the southeastern part of the prospect a residual gravity low anomaly below −1 mgal extends broadly from the line C1 to the line C4. Residual gravity low anomalies are laid in the northwestern part of the line C6 and in the southeastern edge of the line C9.

In the northeastern part small residual gravity low anomalies line up along the base line C0 between the line C13 near the central part and the line C20 in the northeast margin of the prospect. These residual gravity low anomalies correspond to ridges stretching from the Djebel Ech Chied hills to the El Aroussa plain. Though Triassic dolomites with high density are frequently exposed in the ground surface of the ridge areas, the residual gravity low anomalies suggest underlying rock masses of low density related to diapers.

The Bazina Kebira mineral occurrence in the vicinity of the line C4, the Koudiat Soda ore deposit and the Koudiat Tlilette mineral occurrence in the vicinity of the line C17 are located within and in the vicinity of residual gravity low anomalies. The H'Zamel Assoued mineral occurrence in the vicinity of the line C7 and the Koudiat Safra ore deposit lie within and around residual gravity high anomaly.

④First Vertical Derivative Gravity (Figure 27)

The first vertical derivative gravity distribution of the prospect is divided into the southwestern and northeastern parts from the Koudiat Safra ore deposit of the old Sidi Ayed mine such as the gravity distribution. In the northeastern part, the contour of 0 mgal/km runs along the line from the station C12-25 to C20-15 in the direction of ENE-WNW. In the southeastern side of the contour first vertical derivative become low. The contour runs in the northwestern hill side of the contact zone between the Triassic and the Cretaceous systems observed on the ground surface. In the southwestern part, the contour of 0 mgal/km runs complicatedly. Anomalies of first vertical derivative gravity approximately correspond to those of residual gravity.

⑤Cross Section Analysis

In the cross section analysis of the Bazina Kebira prospect, the Cretaceous system is

Lambert X (m)

Lambert Y (m)

N

Koudiat Tiffatt

Koudiat Soda Mine

Koudiat Sarra Mine

Tzamel Assouad

Bazina Kebira

Residual Gravity (Unit: mgal)

-3 -2.6 -2.2 -1.8 -1.4 -1 -0.6 -0.2 0.2 0.6 1 1.4 1.8

0 500 1000 1500 2000

Figure 26

Residual gravity map
in Bazina Kebira prospect

Scale 1 : 30,000

March, 2001

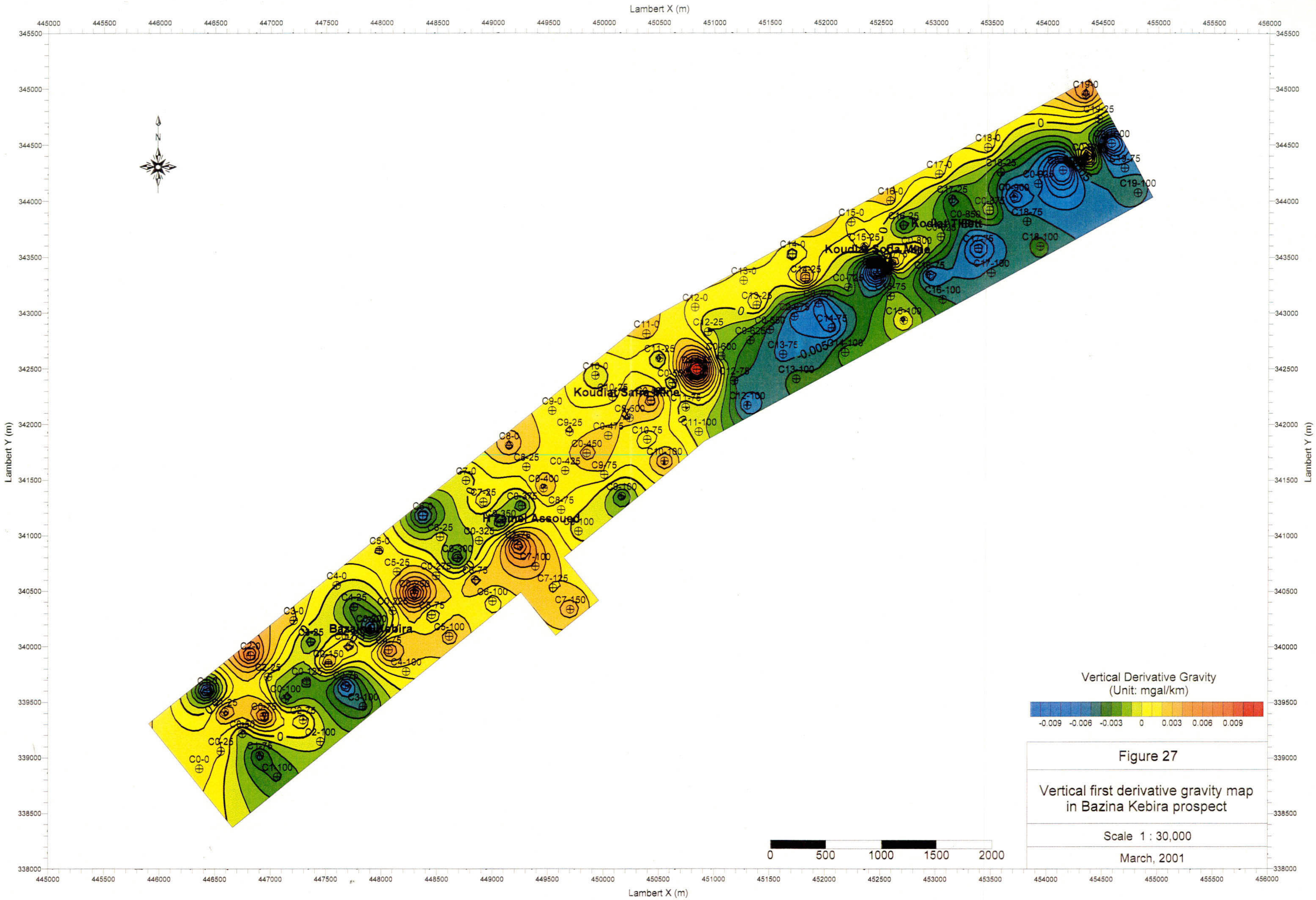

Figure 27

Vertical first derivative gravity map in Bazina Kebira prospect

Scale 1 : 30,000

March, 2001

suppose a gravity basement with density difference of 0.00 g/cm^3. It is assumed that above the gravity basement the Triassic systems with low density difference of -0.10 g/cm^3 overlies in the northwestern Djebel Ech Chied hills side, the Tertiary systems with low density difference of -0.15 g/cm^3 and the Quaternary systems with low density difference of -0.30 g/cm^3 in the southeastern El Arrousa plain side. The result of each profile is describes below.

・Cross Section C0 (Figure 28)

This is a longitudinal section crosscutting the prospect along the base line from the southwest to the northeast through 5 mineral occurrences. In the southwestern part of the line the low density layer with density difference of -0.10 g/cm^3 which may reflect Triassic sandstones and mudstones including gypsums is thick, the thickness of the layer increases nearly 1,000 m between the station C0-1000 and 3000 including the Bazina Kebira mineral occurrence. The relative high-density zone with density difference within the low density layer is supposed the parts dominated by dolomite of the Triassic systems. Triassic low density layers also lie in the areas between C0-3500 and 4300, C0-5800 and 7600, and the vicinity of the northeastern margin. Six thin layers with relatively density difference of -0.15 g/cm^3 lower than the Triassic systems are overlying from the central part to the northeast part.

The gravity basement rises and the boundaries with overlying low density layers suggest the fault structures in the vicinity of the mineral occurrences except for the Bazina Kebira in the southwest part of the prospect. The fact that the low density layers corresponded and the gravity basement vertically bounded to an elevation of approximately -500 m in the southwest side of the H'Zamel Assoued mineral occurrence and below the Koudiat Soda working. The Bazina Kebira mineral occurrence is located in the central part of the thick layer with density difference of -0.10 g/cm^3 that is corresponded to the Triassic systems.

・Cross Section C4 (Figure 29)

This is the southwestern cross section, running from the northwest to the southeast. The low density layer with density differences of –0.2 through 0.0 g/cm^3 in the northwestern hill side from the C4-70 in the central part of the line lie, and the gravity basement rises in the southeastern plain side. The low density layer overthrusts above the gravity basement towards the plain side. Within low density layer the lower density zone with density difference of –0.20 g/cm^3 is located in the vicinity of the C4-50 in the central part. The relatively high density zone in the marginal area of the line can be reflected the Triassic dolomite. The low density overburden with density difference of –0.30 g/cm^3, which is corresponded to the Quaternary systems, is overlying the gravity basement.

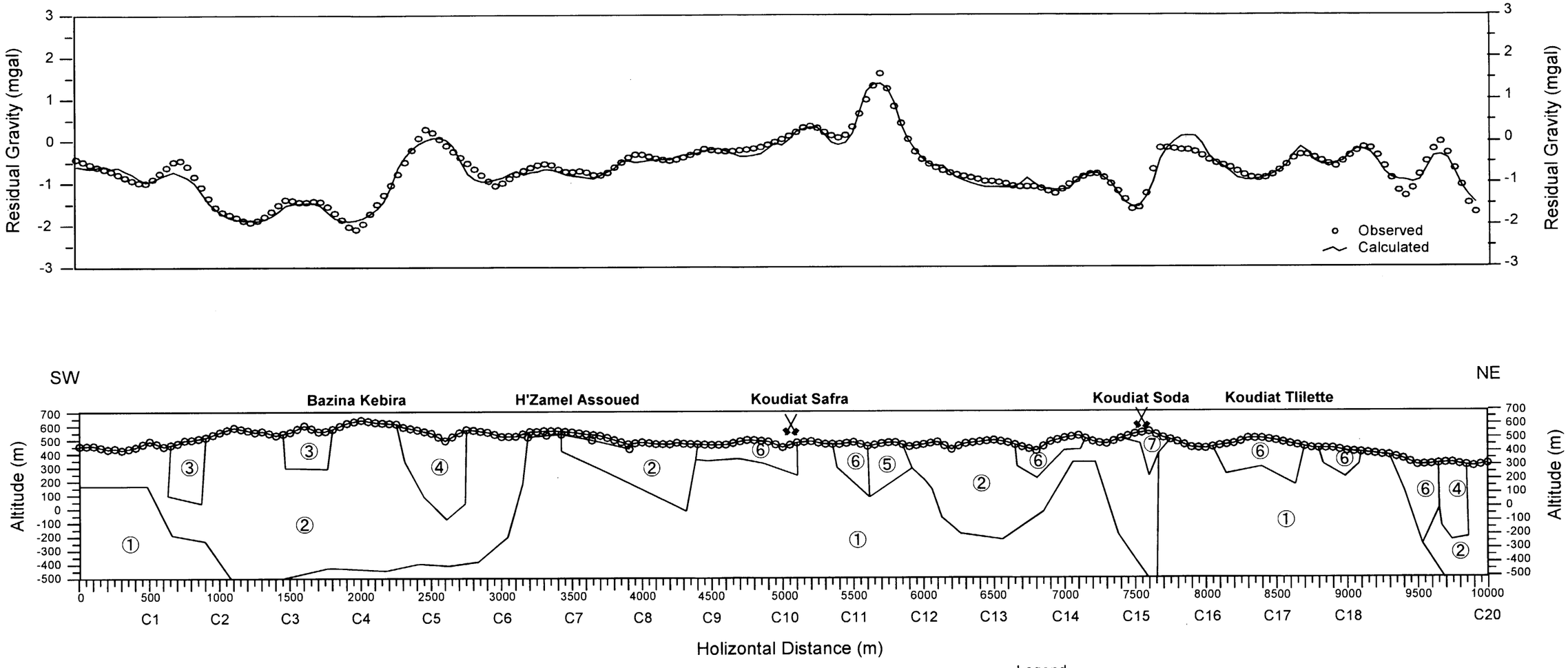

Legend

No.	$\Delta\rho$ (g/cm³)
①	0.00
②	-0.10
③	0.00
④	0.10
⑤	0.20
⑥	-0.15
⑦	-0.25

Figure 28

Result of 2-D Gravimetric analysis (Line C0)

Scale : 30,000

March, 2001

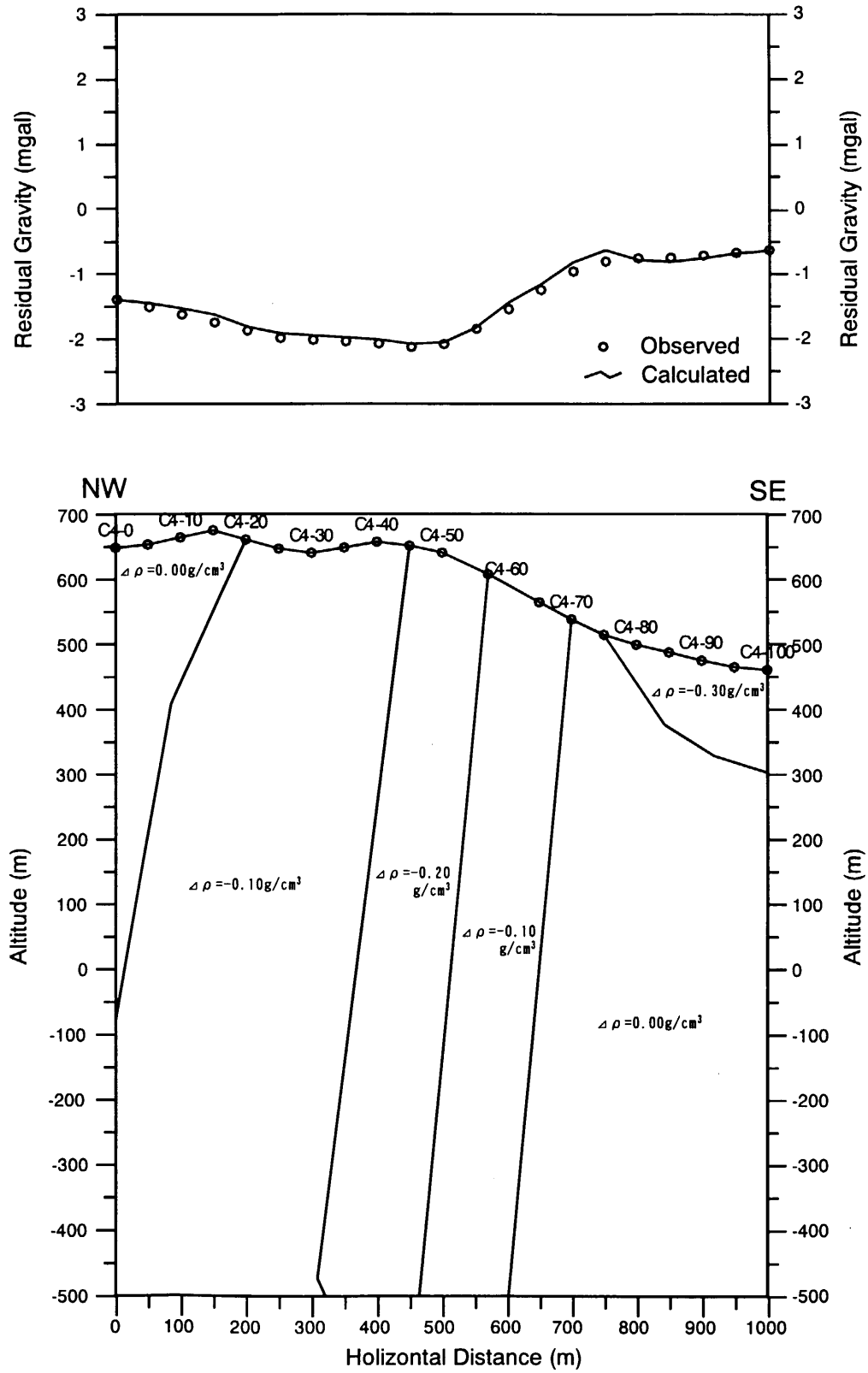

Figure 29
Result of 2-D Gravimetric analysis (Line C4)
Scale : 10,000
March, 2001

・Cross Section C6 (Figure 30)

This section runs in the northeast of 1km apart from the section C4 parallel. Such as the cross section C4 the low density layer with density difference of –0.10 to 0.0 that is corresponded the Triassic systems overthrust in the vicinity of the C6-60 in the central part to the gravity basement in the southeastern plain side. The upper-most layer between the C6-10 and 40 in the northwestern part of the section indicates relatively high density with density difference of 0.0 g/cm^3 and is corresponded to the Triassic dolomite.

・Cross Section C7 (Figure 31)

This section runs in the northeast of 500m apart from the section C6 parallel through the H'Zamel Assoued mineral occurrence. Such as the section C4 and C6 the low density layer with density difference of –0.20 to 0.0 that is corresponded the Triassic systems overthrust in the vicinity of the C7-70 in the central part to the gravity basement in the southeastern plain side. The low density layer includes the relatively lower zone of –0.20 g/cm^3 and the higher zone of 0.0 g/cm^3. The low density overburden with density difference of –0.15 g/cm^3, which may reflect the Tertiary systems, is overlying the gravity basement.

・Cross Section C9 (Figure 32)

This section crosscuts the central part of the prospect from the northwest to the southeast. The gravity basement expands almost cross-section except for the surface layer with low density difference of –0.10 g/cm^3 between C9-5 and 40 in the northwestern part, which is corresponded to the Tertiary system, and the overburden with low density difference of –0.30 g/cm^3 in the southwestern marginal part, which can reflect the Quaternary system. The result don't agree with the geological proof which the boundary between the Triassic systems and the Cretaceous systems is runs in the central part such as the section C4 through C7. It is supposed that the Triassic dolomite zone with the relatively higher density make the boundary ambiguous.

・Cross Section C10 (Figure 33)

This section crosscuts the Koudiat Safra working in the central part of the prospect from the northwest to the southeast. Such as the section C4 through C7 the low density layer with density difference of -0.10 g/cm^3, which is corresponded to the Triassic systems, lies in the northwestern hill side from the C-35 in the central part of the line. The gravity structure in the southeastern side of the low density layer is principally two-layered, composed of a low density layer with density difference of -0.15 g/cm^3, which is thick ranging from 100 to 150m and can reflect the Tertiary systems, and the underlying gravity basement. The fact that Cretaceous sandstone and mudstone distribute on the ground surface around the Koudiat

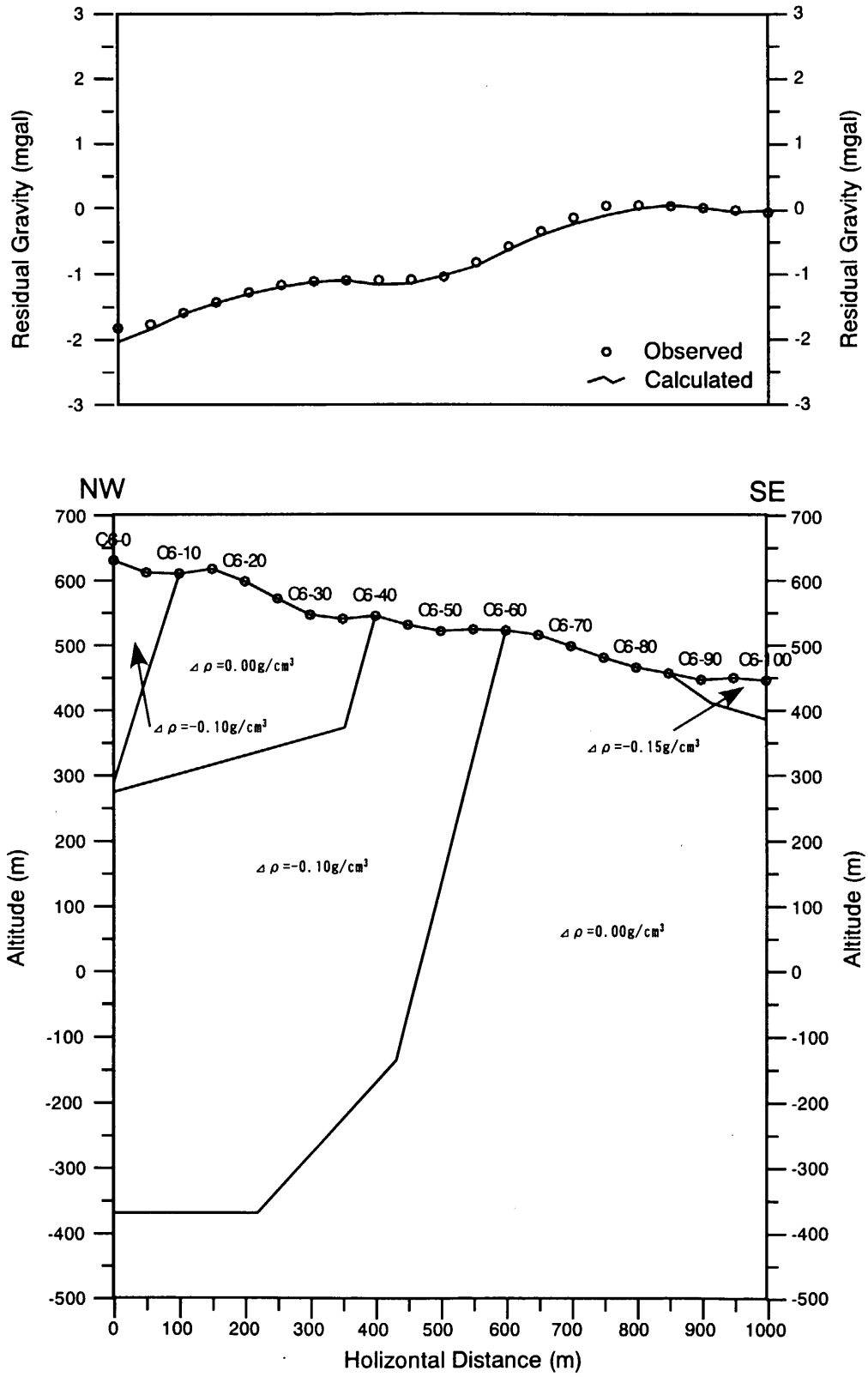

Figure 30
Result of 2-D Gravimetric analysis (Line C6)
Scale : 10,000
March, 2001

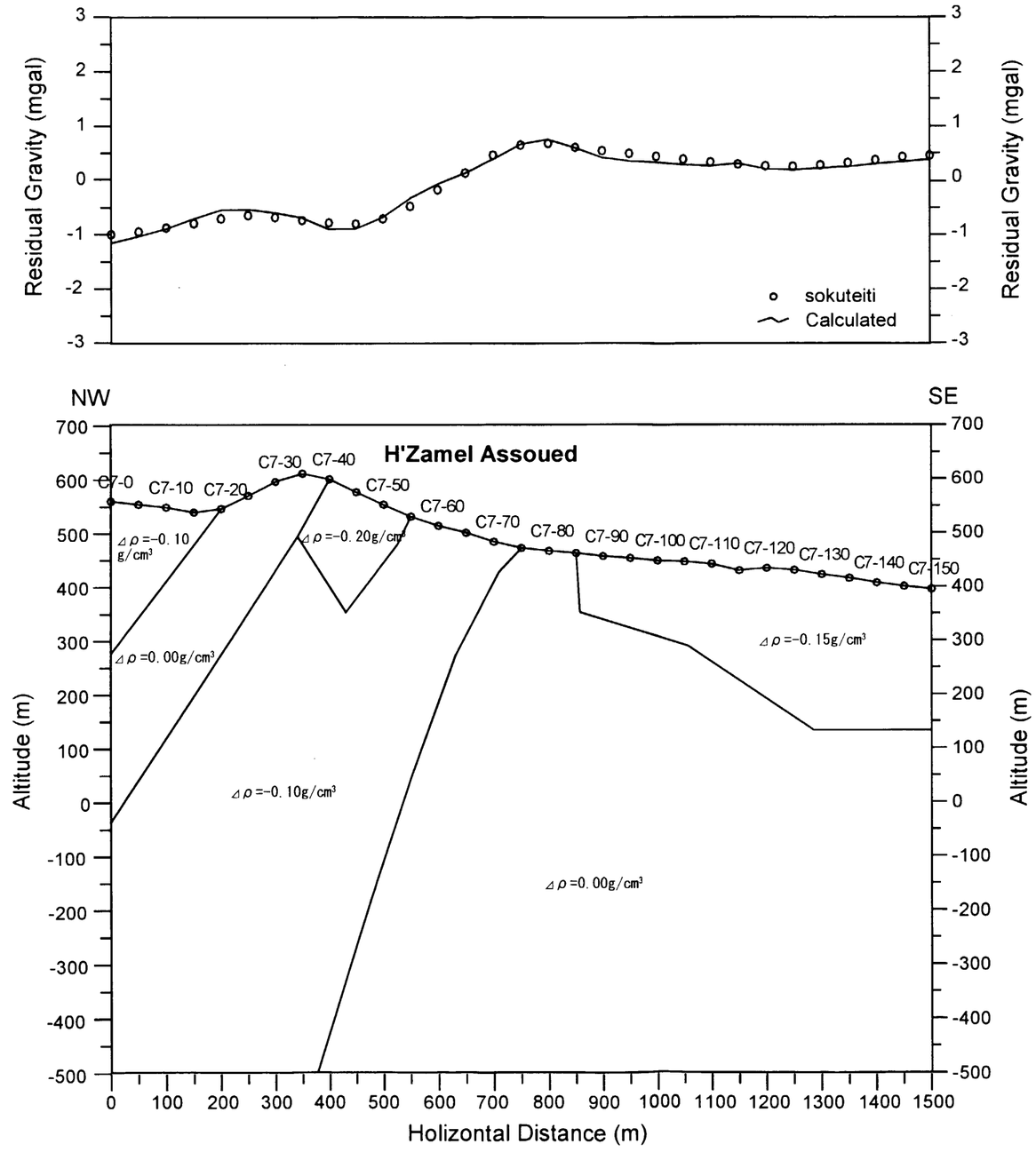

Figure 31
Result of 2-D Gravimetric analysis (Line C7)
Scale : 10,000
March, 2001

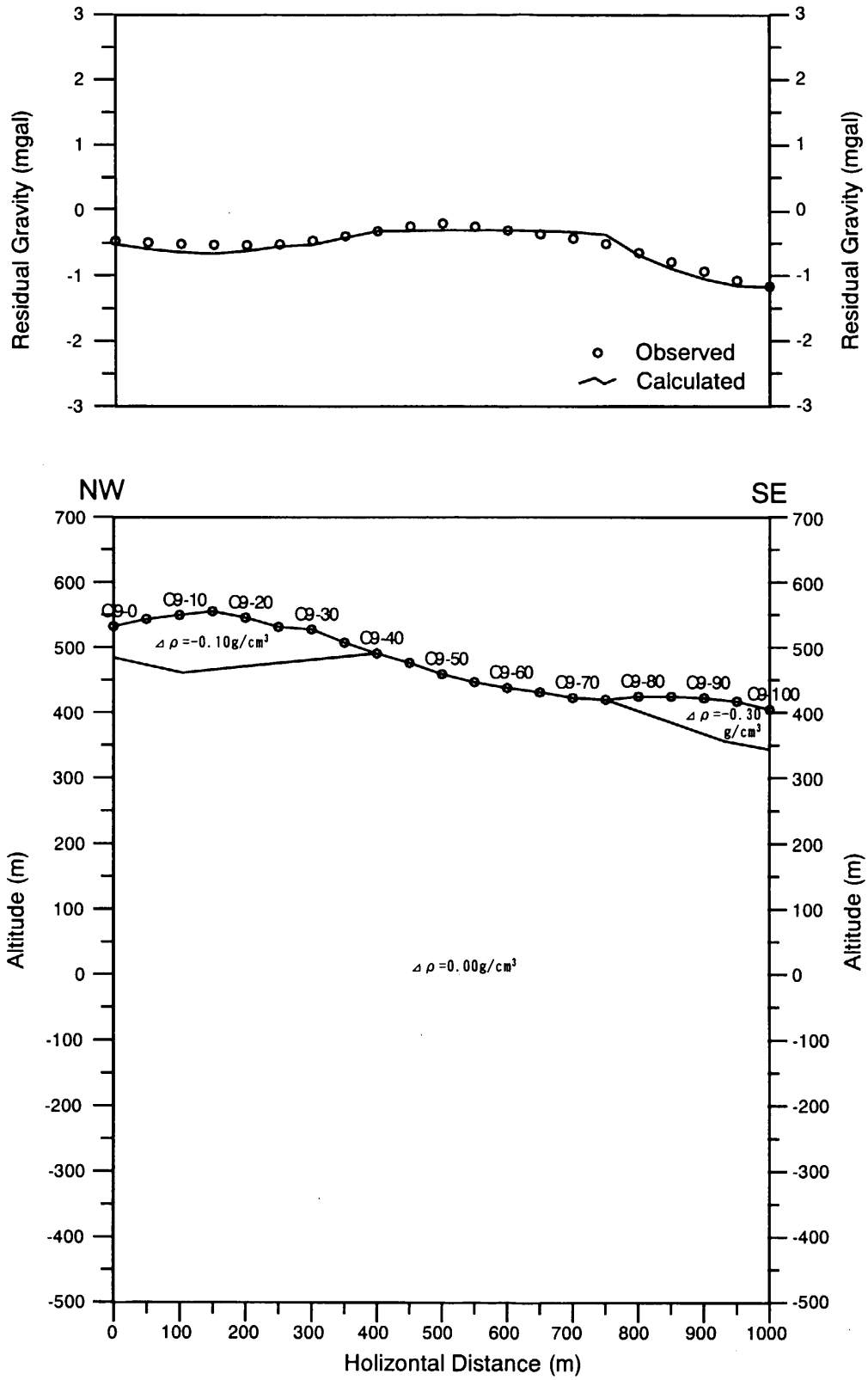

Figure 32
Result of 2-D Gravimetric analysis (Line C9)
Scale : 10,000
March, 2001

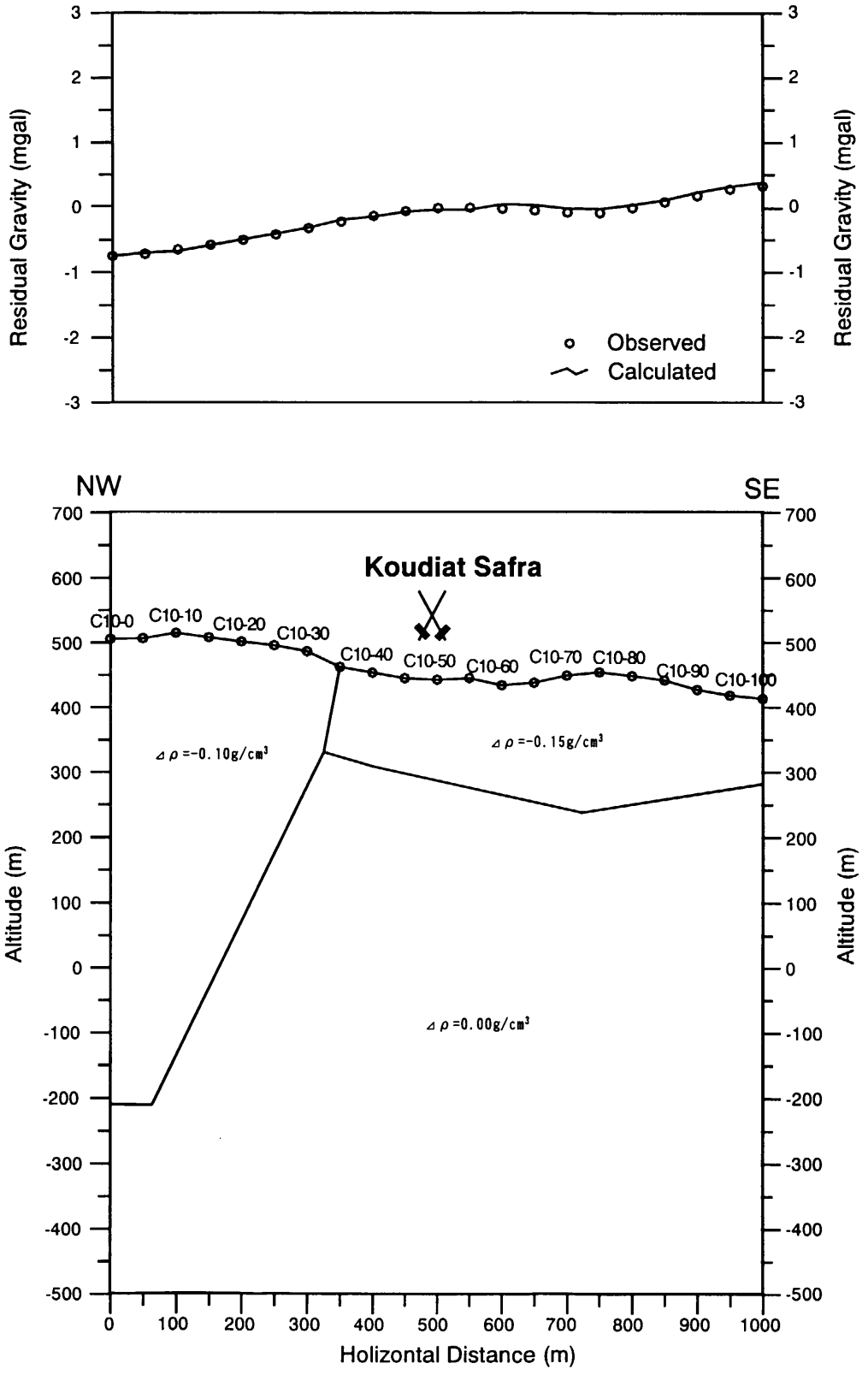

Figure 33
Result of 2-D Gravimetric analysis (Line C10)
Scale : 10,000
March, 2001

Safra working in the vicinity of the boundary with the Triassic system suggest the difficulty of discrimination between the Cretaceous rock less density than limestone and the Tertiary system.

・Cross Section C11 (Figure 34)

This section runs in the northeast of 500m apart from the section C10 parallel. Such as the section C10 the low density layer with density difference ranging from -0.10 to 0.00 g/cm^3, which is corresponded to the Triassic systems, lies in the northwestern hill side from the C11-60 in the central part of the line, and the low density overburden with density difference of -0.15 g/cm^3, which can reflect the Tertiary systems, overlies the gravity basement in the southeastern side. Thickness of the low density overburden ranges from 600 to 700 m, it is thicker than that of the section C10.

・Cross Section C14 (Figure 35)

This section crosscuts the northeastern part of the prospect from the northwest to the southeast. The boundary of the gravity basement corresponded to the Cretaceous systems with the low density layer with density difference ranging between -0.10 and 0.00 g/cm^3, which reflect the Triassic systems, in the vicinity of the C14-90 in the central part of the line suggest the fault structure. The gravity basement is also recognized in the deep zone of the northwestern part. It is supposed that the deep gravity basement is overlaid the rock mass with same density difference. The rock mass isn't corresponded to gravity basement, but Triassic dolomite. The lower surface layer with density difference of -0.15 g/cm3, which may reflect the Tertiary system, overlies thick above the Triassic systems between C14-30 and 80 in the central part of the section.

・Cross Section C15 (Figure 36)

This section runs in the northeast of 500m apart from the section C14 parallel through the Koudiat Soda working. Such as the section C14 the boundary of the gravity basement and the low density layer with density difference of -0.10 g/cm^3, which reflect the Triassic systems. The gravity basement is also recognized in the deep zone of the northwestern part. The density difference of the low density surface layer between the C15-30 and 80 including Koudiat Soda working in the central part is -0.25g/cm^3 lower than the section C14.

・Cross Section C16 (Figure 37)

This section runs in the northeast of 500m apart from the section C15 parallel. The low density layer with density difference ranging from -0.15 to -0.10 g/cm^3, which is corresponded to the Tertiary systems, almost covers the section except for the gravity basement exposed on the ground surface between C16-50 and 60 in the central part of the section. The lower rock

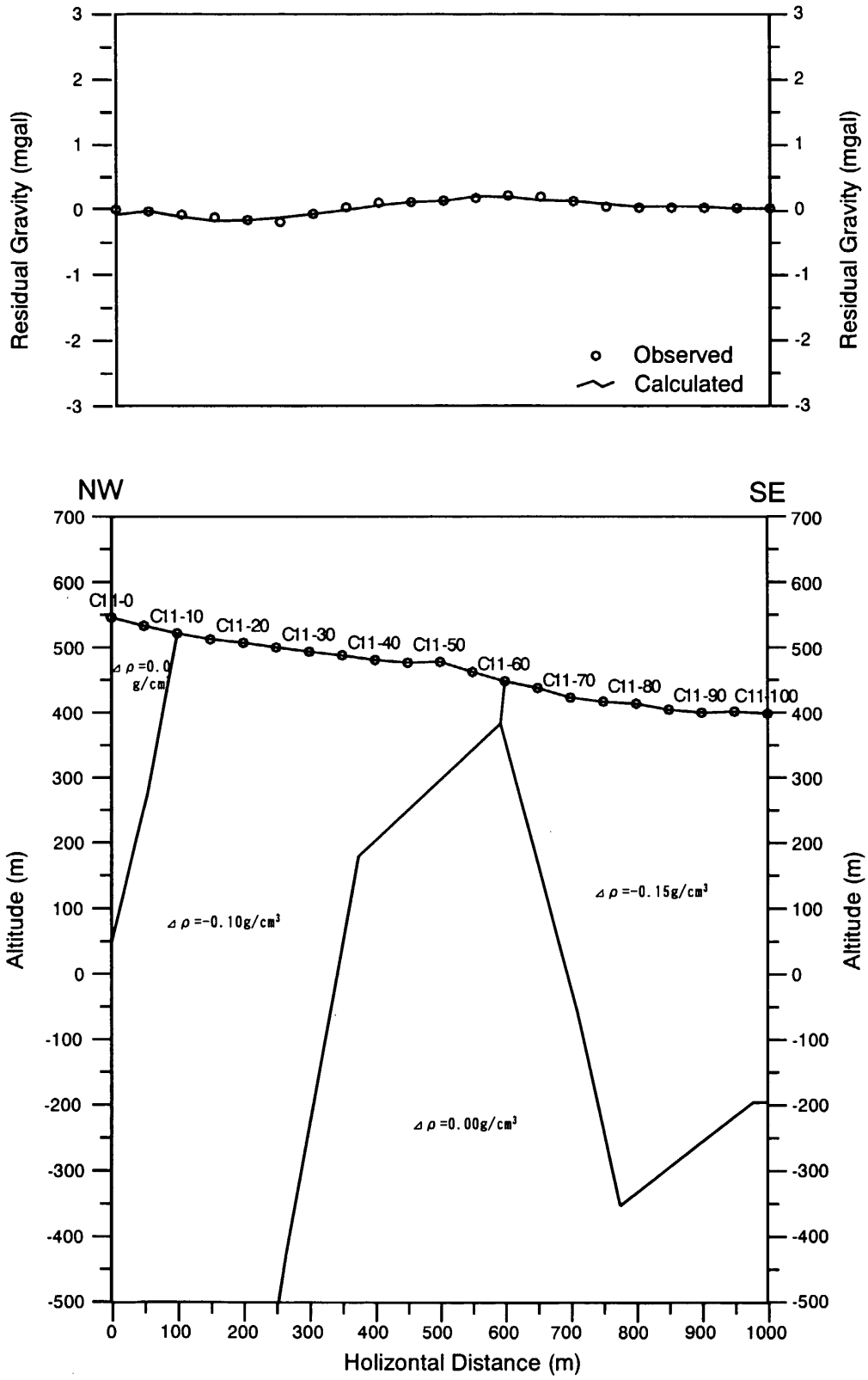

Figure 34
Result of 2-D Gravimetric analysis (Line C11)
Scale : 10,000
March, 2001

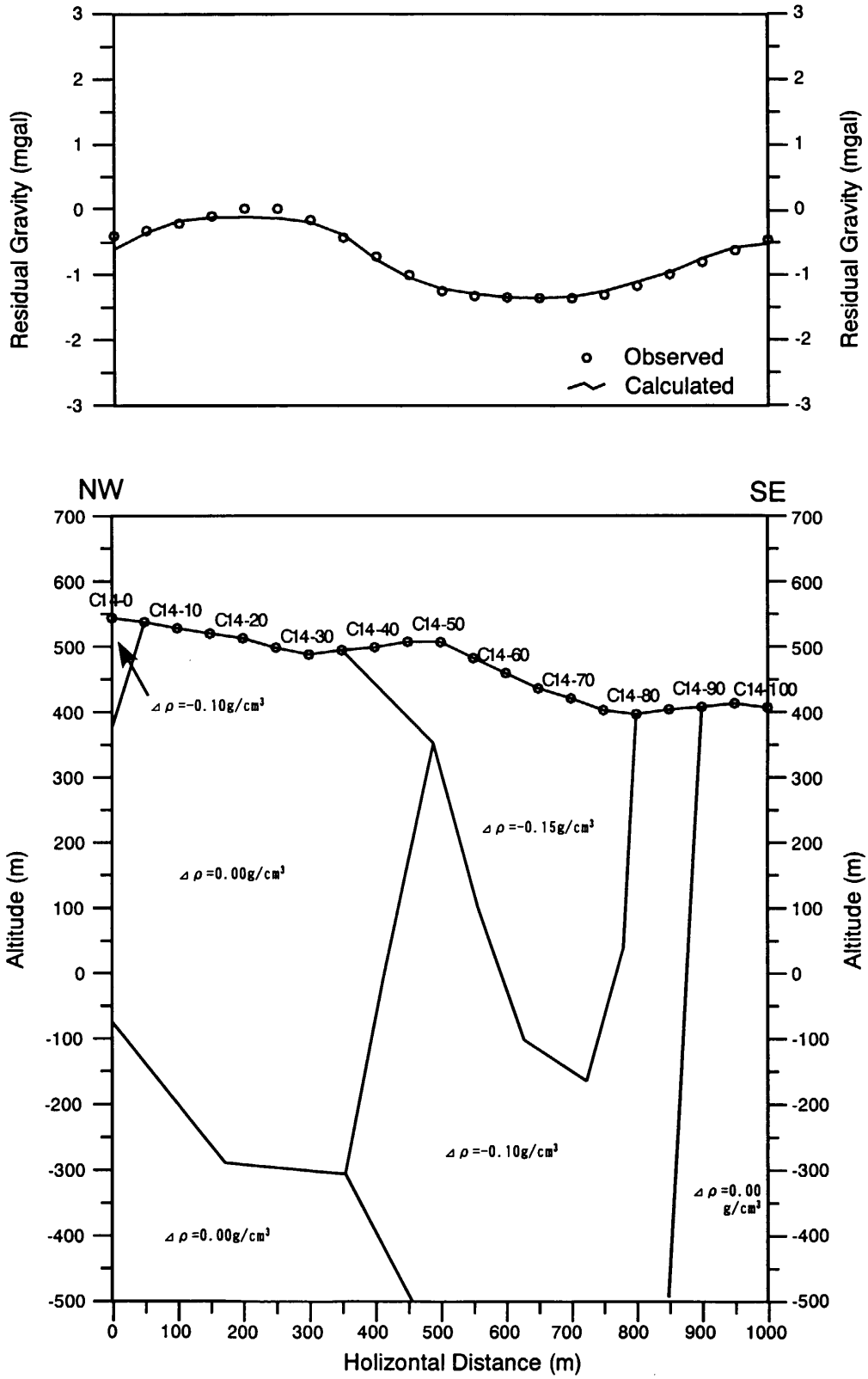

Figure 35
Result of 2-D Gravimetric analysis (Line C14)
Scale : 10,000
March, 2001

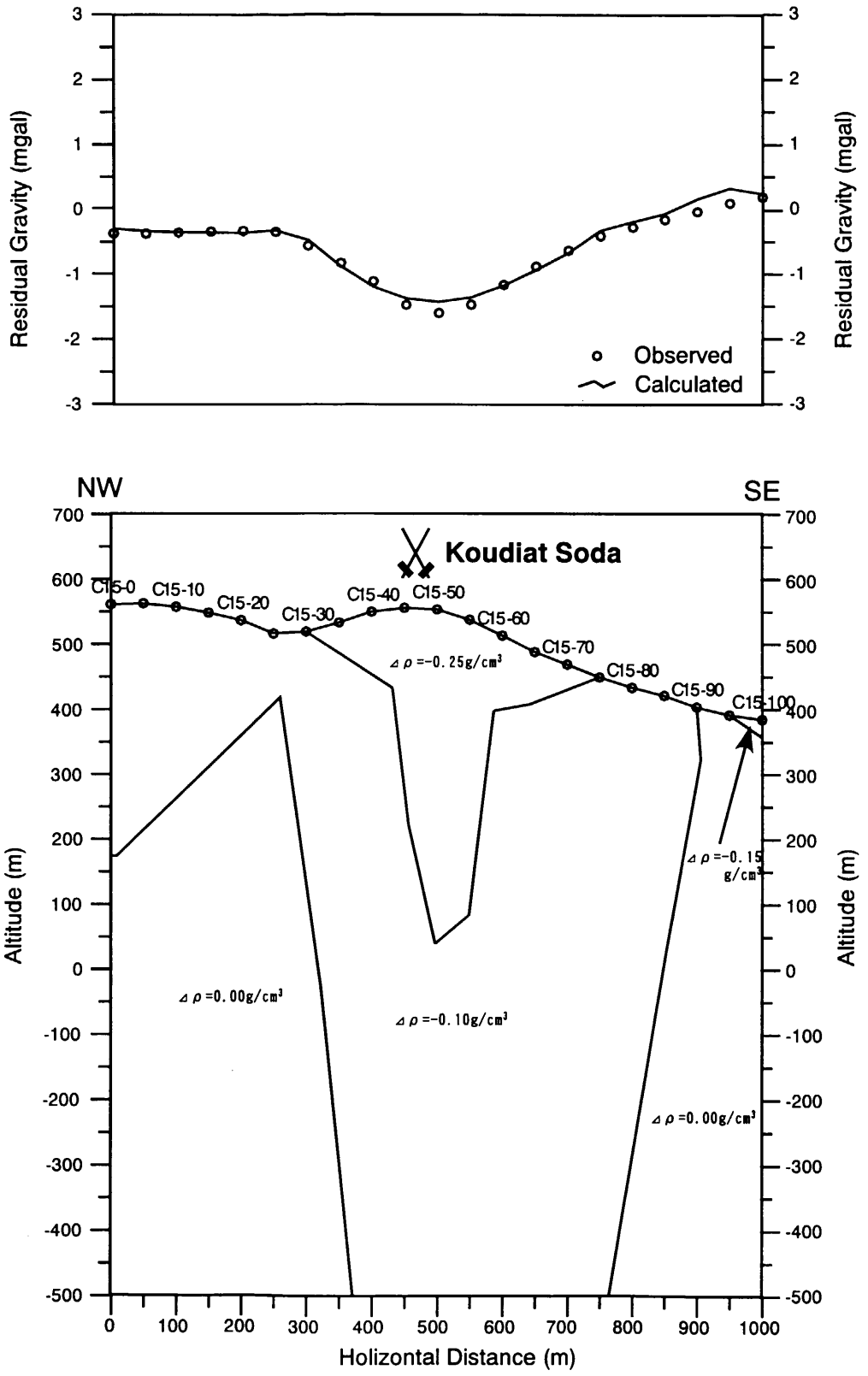

Figure 36
Result of 2-D Gravimetric analysis (Line C15)
Scale : 10,000
March, 2001

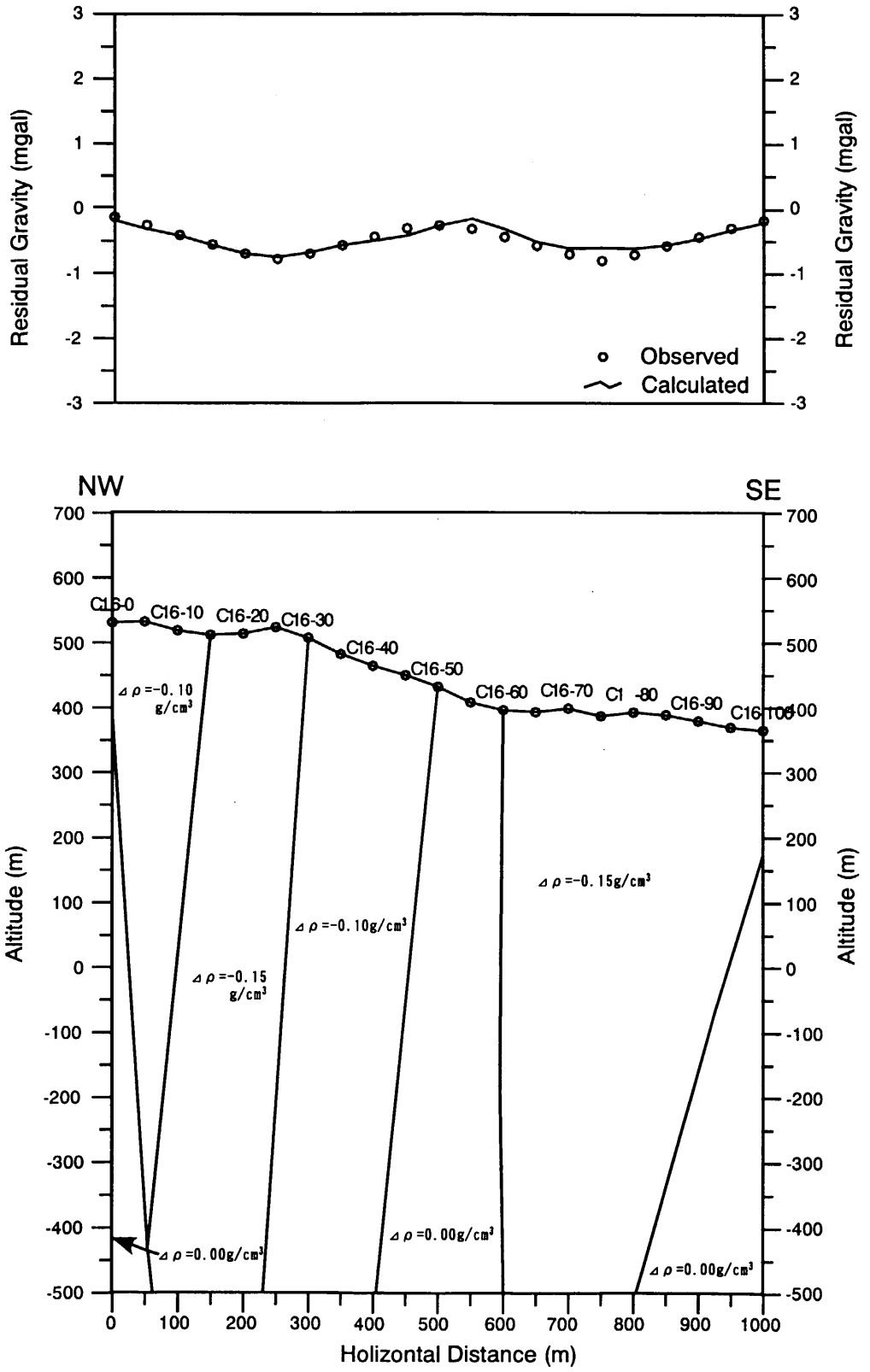

Figure 37
Result of 2-D Gravimetric analysis (Line C16)
Scale : 10,000
March, 2001

mass with the density difference of -0.15 g/cm^3 lies from the C16-15 to 30 in the northwestern part. The boundaries of the gravity basement of the central part with the low density Tertiary layers suggest the complicated geological structure on the section such as the fault structure.

・Cross Section C17 (Figure 38)

This section runs in the northeast of 500m apart from the section C16 parallel through the Koudiat Tlilette mineral occurrence. The gravity basement lies deeply in the northwestern part, and it is exposed on the ground surface between C17-55 and 60 in the central part.

A low density layer with density difference of -0.15 to -0.10 g/cm^3, which is corresponded to the Tertiary systems, is underlain the gravity basement in the northwestern part and the other low density layer lies in the southeastern part. The vertical boundaries of rock masses in the both sides of the Koudiat Tlilette fall down in the vicinity of the C17-20 and the 60, and suggest fault structures.

⑥Interpreted gravity map

The interpreted gravity map composed of the valid anomalies of residual gravity, the 0 mgal/km contour of first vertical differential gravity and the contours of Bouguer anomaly overlaid geological maps shown in Figure 39.

In the Bouguer anomaly the zones of the Triassic systems indicate the high anomalies. On the contrary, they show the low anomalies in the residual gravity such as the northwestern part of the prospect. The fact that the diapirs forming the Djebel Ech Chied hills are composed of rock masses with low density leads the suggestion that the residual gravity represents locations of the diapirs. It is supposed that the high Bouguer anomalies suggest deeper structure lifting diapir up.

Such as the northeastern part, the contour line of 0 mgal/km in the first vertical differential gravity runs parallel to the southeast edge of the Triassic systems on the geological map, closes to the northwestern hill side. The fact suggest that the Triassic systems overhung from the Djebel Ech Chied hills towards the El Arrousa plain and the boundary in the subsurface is located closer to the hill side than on the ground surface. This suggestion is supported that the Triassic systems overthrust the gravity basement towards the plain side.

The Bazina Kebira mineral occurrence, the H'Zamel Assoued mineral occurrence, the Koudiat Soda working and the Koudiat Tlilette mineral occurrence in the high altitude areas are located and in the marginal zones of the residual gravity low. There is no valid anomaly of residual gravity around the Koudiat Safra. Though such low anomalies are recognized in the southwestern end and the northeastern end of the prospect, unknown ore deposits could not be expected geologically because of the lack of the cretaceous systems.

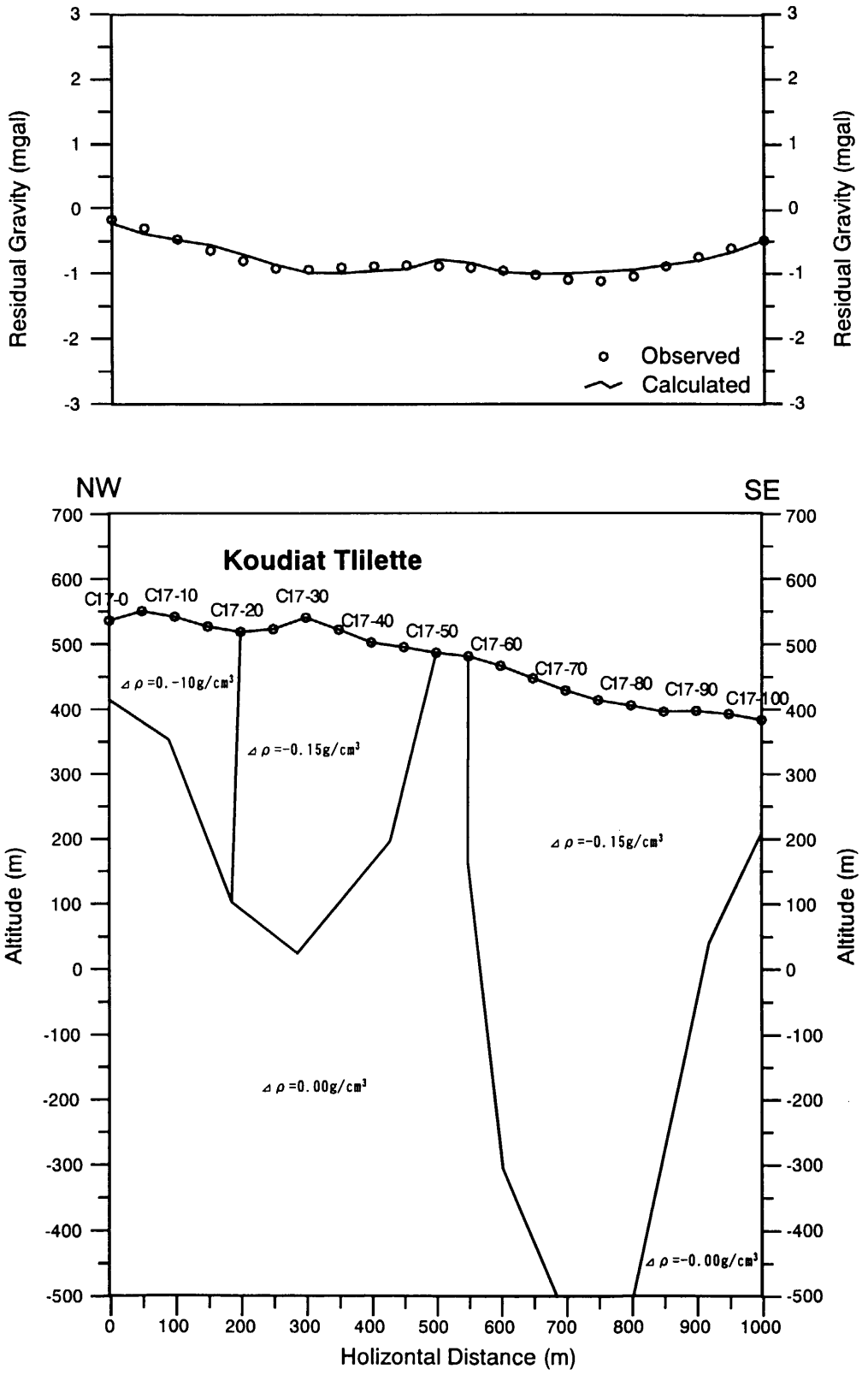

Figure 38
Result of 2-D Gravimetric analysis (Line C17)
Scale : 10,000
March, 2001